INTERNATIONAL JOURNAL FOR NUMERICAL METHODS IN ENGINEERING
Int. J. Numer. Meth. Engng 2015; **102**:933–965
Published online 15 August 2014 in Wiley Online Library (wileyonlinelibrary.com). DOI: 10.1002/nme.4747

A parameterized-background data-weak approach to variational data assimilation: formulation, analysis, and application to acoustics

Yvon Maday[2], Anthony T. Patera[1], James D. Penn[1] and Masayuki Yano[1,*,†]

[1]*Department of Mechanical Engineering, Massachusetts Institute of Technology, 77 Massachusetts Avenue, Cambridge, MA 02139, USA*
[2]*Laboratoire Jacques-Louis Lions, Université Pierre et Marie Curie, 4 Place Jussieu, 75005 Paris, France*

SUMMARY

We present a parameterized-background data-weak (PBDW) formulation of the variational data assimilation (state estimation) problem for systems modeled by partial differential equations. The main contributions are a constrained optimization weak framework informed by the notion of experimentally observable spaces; *a priori* and *a posteriori* error estimates for the field and associated linear-functional outputs; weak greedy construction of prior (background) spaces associated with an underlying potentially high-dimensional parametric manifold; stability-informed choice of observation functionals and related sensor locations; and finally, output prediction from the optimality saddle in $\mathcal{O}(M^3)$ operations, where M is the number of experimental observations. We present results for a synthetic Helmholtz acoustics model problem to illustrate the elements of the methodology and confirm the numerical properties suggested by the theory. To conclude, we consider a physical raised-box acoustic resonator chamber: we integrate the PBDW methodology and a Robotic Observation Platform to achieve real-time *in situ* state estimation of the time-harmonic pressure field; we demonstrate the considerable improvement in prediction provided by the integration of a best-knowledge model and experimental observations; we extract, even from these results with real data, the numerical trends indicated by the theoretical convergence and stability analyses.

Received 30 March 2014; Revised 14 June 2014; Accepted 24 June 2014

KEY WORDS: variational data assimilation; parameterized partial differential equations; model order reduction; design of experiment; robotic data acquisition; acoustics

1. INTRODUCTION

The best-knowledge mathematical model of a physical system is often deficient because of limitations imposed by available knowledge, calibration requirements, and computational solution costs. Accurate prediction thus requires the incorporation of experimental observations in particular to accommodate both anticipated, or parametric, uncertainty and unanticipated, or nonparametric, uncertainty. We present in this paper a parameterized-background data-weak (PBDW) formulation of the variational data assimilation problem for physical systems modeled by PDEs.

Our goal is state estimation. We seek an approximation, $u^*_{\cdot,\cdot}$, to the true field u^{true}, over some spatial domain of interest, Ω. (The state estimate subscript placeholders anticipate two discretization parameters to be introduced shortly.) We shall afford ourselves two sources of information: a best-knowledge (bk) mathematical model in the form of a parameterized PDE defined over Ω (or more generally, a domain Ω^{bk}, which includes Ω) and M experimental observations of the true field,

*Correspondence to: Masayuki Yano, 77 Massachusetts Ave, Rm 3-237, Cambridge, MA 02139, USA.
†E-mail: myano@mit.edu

interpreted as the application of prescribed observation functionals [1] ℓ^o_m, $m = 1, \ldots, M$, to u^{true}. We shall assume that the true field is deterministic and time independent (or time harmonic); we shall further assume, in this first paper, that the observations are noise free.

Given a parameter value μ in a prescribed parameter domain $\mathcal{D}$, we denote the solution to our best-knowledge parameterized PDE as $u^{\text{bk},\mu}$. We may then introduce the parametric manifold associated with our best-knowledge model as $\mathcal{M}^{\text{bk}} \equiv \{u^{\text{bk},\mu} | \mu \in \mathcal{D}\}$. We intend, but we shall not assume, that u^{true} is close to the manifold: there exists a $\tilde{\mu} \in \mathcal{D}$ such that u^{true} is well approximated by $u^{\text{bk},\tilde{\mu}}$. We shall require that, *in any event*, our state estimate $u^*_{\cdot,\cdot}$, now denoted $u^*_{\cdot,M}$, shall converge to u^{true} in the limit of many (noise-free) observations, $M \to \infty$.

To provide a more concrete point of reference, we instantiate the terms introduced earlier for the problem we shall consider in this paper. The physical system is a raised-box acoustic resonator chamber: the state we wish to estimate is the time-harmonic (complex) pressure field; the domain of interest Ω is the interior of the raised box, or resonator chamber; the observation functionals are averages over the face of a microphone placed at different positions $x^c_m \in \Omega$, $m = 1, \ldots, M$. The best-knowledge model is the Helmholtz PDE of acoustics: the domain Ω^{bk} is a large hemispherical dome that includes Ω; the boundary conditions comprise a speaker Neumann model as well as far-field radiation; the (here, singleton) parameter μ, which appears in the PDE and boundary conditions, is the wavenumber (or nondimensional frequency) of the time-harmonic pressure; the parameter domain is $\mathcal{D} = [0.5, 1.0]$ (roughly 1000–2000 Hz in dimensional terms).

We shall first motivate the PBDW formulation from a perspective directly relevant to the theme of this special issue, model order reduction. For concreteness, we consider the particular model-reduction approach, which we shall subsequently pursue in this particular paper, the certified reduced basis (CRB) method; however, other approaches are also possible and are briefly summarized later. In this context, the point of departure is the parametric manifold $\mathcal{M}^{\text{bk}}$ associated with the solutions of our best-knowledge PDE. (The CRB approach requires for computational expediency that the parameterized PDE be affine in functions of the parameter: often, inspection suffices to verify this condition; more generally, the empirical interpolation method [2] provides an (approximate) construction.) We shall then revisit the PBDW formulation, but now from the related perspectives of data interpolation, least-squares approximation, and variational data assimilation. In this context, the point of departure is the minimization of the misfit between model predictions and experimental observations.

We briefly summarize the ingredients of the CRB approach [3]: construction of a Lagrange [4] approximation space $\mathcal{Z}_N$ as the span of N snapshots, $\hat{\mu}_n \in \mathcal{D} \to u^{\text{bk},\hat{\mu}_n}$, $n = 1, \ldots, N$, on the parametric manifold $\mathcal{M}^{\text{bk}}$; approximation of the solution of the PDE, $u^{\text{bk},\mu}$, for any parameter value $\mu \in \mathcal{D}$, as the Galerkin projection over $\mathcal{Z}_N$, $u^{\text{bk},\mu}_N$; development of *a posteriori* error estimates $\Delta^{\text{bk},\mu}_N$—in fact, often *bounds*—for the error $\|u^{\text{bk},\mu} - u^{\text{bk},\mu}_N\|$ in terms of the dual norm of the residual and corresponding stability constants; formulation of construction–evaluation procedures, which permit rapid computation of the CRB approximation and *a posteriori* error bound in the limit of many queries $\mu \to u^{\text{bk},\mu}_N$, $\Delta^{\text{bk},\mu}_N$; application of weak greedy sampling procedures, which exploit the construction–evaluation procedure to efficiently identify quasi-optimal (snapshots and hence) approximation spaces $\mathcal{Z}_N$ relative to the Kolmogorov gold standard [5]; and finally, deployment in an offline–online computational framework such that the online stage—the response to each new parameter request—invokes only inexpensive evaluations. The method is relevant in the real-time context or the many-query context in which the offline (and construction) costs are respectively irrelevant or amortized.

We now turn to real physical systems, for example, the raised-box acoustic resonator, which we shall study in the concluding section of this paper. For such a physical system and associated best-knowledge model, we may propose to approximate u^{true} by $u^{\text{bk},\tilde{\mu}}_N$, the CRB approximation of the closest element on the best-knowledge manifold $\mathcal{M}^{\text{bk}}$. We identify two impediments. First, in general, we will not know $\tilde{\mu}$ *a priori*: (anticipated) parametric uncertainty may arise for example because of imperfect control of ambient temperature and thus sound speed. Hence, we cannot instantiate our weak form, and as a result, we are simply not able to apply Galerkin projection to determine $u^{\text{bk},\tilde{\mu}}_N$. Second, we cannot control the *model* error $\inf_{\tilde{\mu}\in\mathcal{D}} \|u^{\text{true}} - u^{\text{bk},\tilde{\mu}}\|$: unanticipated nonparametric uncertainty may arise for example because of uncharacterized impedances on the

DOI: 10.1002/nme

walls of the resonator chamber. In short, CRB approximation assumes, often quite unrealistically, that our best-knowledge mathematical model reflects complete knowledge of the physical system.

Data can provide the necessary closure for both the parametric and nonparametric sources of uncertainty. In particular, we first write our state estimate $u^*_{N,M}$ as the sum of two contributions, $u^*_{N,M} \equiv z^*_{N,M} + \eta^*_{N,M}$. The first contribution to $u^*_{N,M}$, $z^*_{N,M} \in \mathcal{Z}_N$, is the 'deduced background estimate', which represents anticipated uncertainty; $\mathcal{Z}_N$ is now interpreted as a background or prior space that approximates the best-knowledge manifold on which we hope the true state resides. As already discussed, non-zero model error is a virtual certainty, and thus, we cannot realistically assume that u^{true} lies exactly on our best-knowledge manifold, which thus motivates the second contribution to $u^*_{N,M}$. This second contribution to $u^*_{N,M}$, $\eta^*_{N,M} \in \mathcal{U}_M$, is the 'update estimate', which accommodates unanticipated uncertainty; $\mathcal{U}_M$ is the span of the Riesz representations of our M observation functionals [6]. We then search for $\eta^*_{N,M}$ of minimum norm—we look for the smallest correction to the best-knowledge parametric manifold—subject to the observation constraints $\ell^o_m(u^{\text{true}}) = \ell^o_m(u^*_{N,M})$, $m = 1, \ldots, M$. In conclusion, the data affects the projection onto $\mathcal{Z}_N$—in effect serving as test space—and furthermore supplements the best-knowledge model—thus also serving as a supplemental trial space.

The prior or background space $\mathcal{Z}_N$ may be generated from the manifold $\mathcal{M}^{\text{bk}}$ by a variety of model order reduction approaches. We may consider weak greedy procedures as developed in the reduced basis context and summarized earlier in our discussion of the principal CRB ingredients. We may consider classical POD [7]; POD is, relative to weak greedy, more readily implemented, more optimal, and also considerably less efficient in the offline stage. We may consider Taylor spaces [8] and Hermite spaces [9]: expansion of the best-knowledge solution about one or several nominal parameter values in $\mathcal{D}$—in effect, higher-order tangent approximations of the parametric manifold.

We can now relate this PBDW approach to a variety of existing methods. We first consider the model-reduction perspective: PBDW is an approximation method that seeks solution in the reduced basis space $\mathcal{Z}_N \oplus \mathcal{U}_M$ based on projection-by-data, as opposed to projection-by-model in the standard reduced basis method. We next consider the data interpolation perspective: PBDW reduces to the generalized empirical interpolation method (GEIM) [10–12] for $N = M$, any given $\mathcal{Z}_N$; PBDW reduces to Gappy-POD [13, 14] for $M \geq N$, $\mathcal{Z}_N$ generated by a POD, and $u^*_{N,M} \equiv z^*_{N,M}$ (no update correction). We then continue with the least-squares perspective: PBDW reduces to the stable least-squares approximation [15] for $M \geq N$, $\mathcal{Z}_N$ chosen by application-specific basis functions, and $u^*_{N,M} \equiv z^*_{N,M}$ (no update correction); PBDW may also be interpreted, albeit less directly, as linearized structured total least squares [16] for $M \geq N$, $\mathcal{Z}_N$ chosen by Taylor expansion. Finally, and most importantly, PBDW is a *special case* of 3D-VAR variational data assimilation [17] for a parameterized background and a particular choice of (penalized-update) background covariance[‡]; note that in the noise-free case considered in this paper, the variational data assimilation optimization reduces to a constrained estimation problem. We emphasize that PBDW is not a generalization of 3D-VAR, but rather a particular choice for the 3D-VAR constituents.

A particularly important aspect of variational data assimilation, which we incorporate in our framework is the Riesz representation of observation functionals and the associated field update [6]. The former, as first introduced in [6], provides an efficient computational procedure and, in our framework, facilitates *a priori* error analysis; the latter permits accurate state prediction even in situations where the true field is not overly close to, in [6], the baseline solution and, in our framework, the parametric manifold.

The PBDW formulation does provide some new contributions:

(1) Our constrained optimization weak framework informed by the notion of experimentally observable spaces [6, 18]—our update spaces $\mathcal{U}_M$—allows us to incorporate and analyze data within the standard variational setting for PDEs [21]: we can thus develop *a priori*

[‡]It thus follows, by association, that the PBDW formulation can be related to filtering approaches [19, 20].

DOI: 10.1002/nme

error bounds and *a posteriori* error estimates for the field and associated linear-functional 'quantity-of-interest' outputs as a function of N, the dimension of the background space, and M, the number of experimental observations.

(2) The *a priori* theory can serve to inform strategies for the efficient identification of optimal observation functionals—and hence (for localized observation functionals) optimal sensor placement. Different optimality criteria may be considered. In this paper, we choose as criterion the stability of the deduced background estimate $z^*_{N,M}$. Our methods are thus related to classical design-of-experiment approaches [22], however with an emphasis on state estimation rather than parameter estimation; in particular, both methods rely on singular-value considerations. We may also consider criteria that balance stability of the background estimate $z^*_{N,M}$ with accuracy of the update estimate $\eta^*_{N,M}$ [23].

(3) We incorporate several important aspects of model order reduction: parameterized best-knowledge model and the associated parametric manifold—rather than a singleton best-knowledge solution—to reflect anticipated uncertainty; efficient weak greedy construction of rapidly convergent prior (background) spaces associated with an underlying potentially high-dimensional parametric manifold; output prediction from the optimality saddle in $\mathcal{O}((N+M)^3)$ operations for N and M anticipated small. (We note that stability will require $M \geqslant N$: a good background space thus reduces not only computational effort but also experimental cost.)

(4) The PBDW formulation offers simplicity and generality: the best-knowledge model appears only in the offline stage and solely in the generation of the space $\mathcal{Z}_N$.

These features will be highlighted in the sections that follow.

We note that projection-by-data—a problem in approximation theory—rather than projection-by-model—a problem in PDE discretization—also has many advantages with respect to the mathematical theory. Projection-by-data can largely eliminate many of the standard requirements of projection-by-model, in particular related to boundary conditions and initial conditions; for example, the domain over which we reconstruct the state, Ω, can be a subset of the best-knowledge spatial domain, Ω^{bk}, and indeed, Ω can even be a low-dimensional manifold in Ω^{bk}. Even more ambitiously, in projection-by-data, we can accommodate norms that may be considerably stronger than the norms required for well-posedness in projection-by-model; furthermore, the greater regularity required by data in these stronger norms can be justified by the application of temporal or spatial filters—in short, by a re-definition of the true field, u^{true}. In subsequent studies, we shall explore further these theoretical generalizations and associated computational extensions and improvements.

We emphasize that in this paper we restrict ourselves to state estimation: the PBDW formulation chooses a best state estimate from $\mathcal{Z}_N$ and $\mathcal{U}_M$ as guided by the constrained minimization statement. Clearly, in many cases, state estimation can be related to parameter estimation [22] and source identification [24]; however, we do not here take the necessary steps to infer from our best state estimate $u^*_{N,M}$ a best parameter estimate $\mu^*_{N,M}$. In particular, in our current paper, μ and $\mathcal{D}$ serve only in the (offline) construction of $\mathcal{Z}_N$: the online stage does not benefit from any prior on the parameter, nor does the online stage provide any posterior for the parameter. However, we note that the PBDW update contribution suggests both a complication and an extension to current parameter estimation approaches: $\|\eta^*_{N,M}\|$ allows us to explore the sensitivity of any given parameter estimate to model error. We pursue this possibility in subsequent papers, in which we shall also consider noisy measurements—another important source of uncertainty in (state and) parameter estimation.

In Section 2, we present the PBDW formulation and associated numerical analysis. In Section 3, we present results for a synthetic Helmholtz problem: we illustrate the elements of the methodology; we confirm the numerical properties suggested by the theory. In Section 4, we present results for a physical raised-box acoustic resonator chamber: we integrate the PBDW methodology and a Robotic Observation Platform to achieve real-time *in situ* estimation of the full pressure field over the resonator chamber.

DOI: 10.1002/nme

2. FORMULATION

2.1. Preliminaries

By way of preliminaries, we introduce notations used throughout this paper. We first introduce the standard $L^2(\Omega)$ Hilbert space over the domain $\Omega \subset \mathbb{R}^d$ endowed with an inner product $(w,v)_{L^2(\Omega)} \equiv \int_\Omega wv dx$ and the induced norm $\|w\|_{L^2(\Omega)} = \sqrt{(w,w)_{L^2(\Omega)}}$; $L^2(\Omega)$ consists of functions $\{w \mid \|w\|_{L^2(\Omega)} < \infty\}$. We next introduce the standard $H^1(\Omega)$ Hilbert space over Ω endowed with an inner product $(w,v)_{H^1(\Omega)} \equiv \int_\Omega \nabla w \cdot \nabla v dx + \int_\Omega wv dx$ and the induced norm $\|w\|_{H^1(\Omega)} \equiv \sqrt{(w,w)_{H^1(\Omega)}}$; $H^1(\Omega)$ consists of functions $\{w \mid \|w\|_{H^1(\Omega)} < \infty\}$. We also introduce the $H^1_0(\Omega)$ Hilbert space over Ω endowed with the $H^1(\Omega)$ inner product and $H^1(\Omega)$ norm; $H^1_0(\Omega)$ consists of functions $\{w \in H^1(\Omega) \mid w|_{\partial\Omega} = 0\}$. We note that, for simplicity, we shall consider the formulation over real-valued field; however, in the subsequent applications that appear in Sections 3 and 4, we shall invoke the corresponding extension to complex-valued fields.

We now introduce a Hilbert space $\mathcal{U}$ over Ω endowed with an inner product $(\cdot,\cdot)$ and the induced norm $\|w\| = \sqrt{(w,w)}$; $\mathcal{U}$ consists of functions $\{w \mid \|w\| < \infty\}$. We assume that $H^1_0(\Omega) \subset \mathcal{U} \subset H^1(\Omega)$. We denote the dual space of $\mathcal{U}$ by $\mathcal{U}'$ and the associated duality paring by $\langle\cdot,\cdot\rangle_{\mathcal{U}'\times\mathcal{U}}$. The Riesz operator $R_\mathcal{U} : \mathcal{U}' \to \mathcal{U}$ satisfies, for each $\ell \in \mathcal{U}'$, $(R_\mathcal{U}\ell, v) = \ell(v)\ \forall v \in \mathcal{U}$. For any closed subspace $\mathcal{Q} \subset \mathcal{U}$, the orthogonal projection operator $\Pi_\mathcal{Q} : \mathcal{U} \to \mathcal{Q}$ satisfies $(\Pi_\mathcal{Q} w, v) = (w,v)\ \forall v \in \mathcal{Q}$. The orthogonal complement of $\mathcal{Q}$ is given by $\mathcal{Q}^\perp \equiv \{w \in \mathcal{U} | (w,v) = 0\ \forall v \in \mathcal{Q}\}$.

2.2. Unlimited-observations statement

We first introduce generic hierarchical background (or prior) spaces

$$\mathcal{Z}_1 \subset \mathcal{Z}_2 \subset \cdots \subset \mathcal{Z}_{N_{\max}} \subset \cdots \subset \mathcal{U};$$

here, the last ellipsis indicates that although in practice we shall consider N at most $N_{\max}$, in principle, we might extend the analysis to an infinite sequence of refinements. We intend, but not assume, that

$$\epsilon_N^{\text{bk}}(u^{\text{true}}) \equiv \inf_{w \in \mathcal{Z}_N} \|u^{\text{true}} - w\| \leqslant \epsilon \quad \text{as} \quad N \to \infty$$

for ϵ an acceptable tolerance. As mentioned in the introduction, the background spaces may be generated from the best-knowledge manifold $\mathcal{M}^{\text{bk}}$ by a variety of model-reduction approaches; the spaces consist of candidate states realized by anticipated, and parameterized, uncertainty in the model. We consider several specific choices in detail in Section 2.7.2.

We are now ready to state the unlimited-observations PBDW minimization statement: find $(u_N^* \in \mathcal{U}, z_N^* \in \mathcal{Z}_N, \eta_N^* \in \mathcal{U})$ such that

$$(u_N^*, z_N^*, \eta_N^*) = \arg \inf_{\substack{u_N \in \mathcal{U} \\ z_N \in \mathcal{Z}_N \\ \eta_N \in \mathcal{U}}} \|\eta_N\|^2 \tag{1}$$

subject to

$$\begin{aligned} (u_N, v) &= (\eta_N, v) + (z_N, v) \quad \forall v \in \mathcal{U}, \\ (u_N, \phi) &= (u^{\text{true}}, \phi) \quad \forall \phi \in \mathcal{U}. \end{aligned} \tag{2}$$

The following proposition summarizes the solution to the minimization problem.

Proposition 1
The solution to the PBDW minimization statement (1) is

$$u_N^* = u^{\text{true}}, \quad z_N^* = \Pi_{\mathcal{Z}_N} u^{\text{true}}, \quad \text{and} \quad \eta_N^* = \Pi_{\mathcal{Z}_N^\perp} u^{\text{true}}.$$

DOI: 10.1002/nme

Proof
We first deduce from $(2)_2$ that $u_N^* = u^{\text{true}}$. We next deduce from $(2)_1$ that $\eta_N^* = u^{\text{true}} - z_N^*$. We then note that, as we wish to minimize $\|\eta_N^*\|$, we must choose $z_N^* = \Pi_{\mathcal{Z}_N} u^{\text{true}}$ such that $\eta_N^* = \Pi_{\mathcal{Z}_N^\perp} u^{\text{true}}$. □

Proposition 1 provides a precise interpretation for u_N^*, z_N^*, and η_N^* and solidifies the interpretation alluded to in the introduction: $u_N^* \in \mathcal{U}$ is the 'state estimate', which in fact is equal to the true state u^{true}; $z_N^* \in \mathcal{Z}_N$ is the 'deduced background', the component of the state formed by the anticipated, and parameterized, uncertainty that lies in the background space $\mathcal{Z}_N$; $\eta_N^* \in \mathcal{Z}_N^\perp$ is the 'update', the component of the state formed by unanticipated, and in some sense nonparametric, uncertainty that lies outside of the background space $\mathcal{Z}_N$. Note that the update η_N^* completes the deficient prior space such that $u^{\text{true}} = u_N^* = z_N^* + \eta_N^*$.

We now derive (simplified) Euler–Lagrange equations associated with the PBDW minimization statement (1). Toward this end, we first introduce the Lagrangian

$$\mathcal{L}(u_N, z_N, \eta_N, v, \phi) \equiv \frac{1}{2}\|\eta_N\|^2 + (u_N - \eta_N - z_N, v) + (u_N - u^{\text{true}}, \phi).$$

Here, $u_N \in \mathcal{U}$, $z_N \in \mathcal{Z}_N$, and $\eta_N \in \mathcal{U}$; $v \in \mathcal{U}$ and $\phi \in \mathcal{U}$ are the Lagrange multipliers. We then obtain the (full) Euler–Lagrange equations: find $(u_N^* \in \mathcal{U}, z_N^* \in \mathcal{Z}_N, \eta_N^* \in \mathcal{U}, v^* \in \mathcal{U}, \phi^* \in \mathcal{U})$ such that

$$\begin{aligned}
(v^*, \delta u) + (\phi^*, \delta u) &= 0 \quad \forall \delta u \in \mathcal{U}, \\
(v^*, \delta z) &= 0 \quad \forall \delta z \in \mathcal{Z}_N, \\
(\eta_N^*, \delta\eta) - (v^*, \delta\eta) &= 0 \quad \forall \delta\eta \in \mathcal{U}, \\
(u_N^* - \eta_N^* - z_N^*, \delta v) &= 0 \quad \forall \delta v \in \mathcal{U}, \\
(u_N^* - u^{\text{true}}, \delta\phi) &= 0 \quad \forall \delta\phi \in \mathcal{U}.
\end{aligned} \tag{3}$$

We readily obtain from $(3)_3$ and $(3)_1$ that $v^* = \eta_N^*$ and $\phi^* = v^* = -\eta_N^*$, respectively; we substitute η_N^* in place of v^* and $-\phi^*$. We in addition note from $(3)_5$ that $u_N = u^{\text{true}}$; we make the substitution to $(3)_4$. The substitutions yield the (simplified) Euler–Lagrange equation associated with the PBDW minimization statement (1): find $(\eta_N^* \in \mathcal{U}, z_N^* \in \mathcal{Z}_N)$ such that

$$\begin{aligned}
(\eta_N^*, q) + (z_N^*, q) &= (u^{\text{true}}, q) \quad \forall q \in \mathcal{U}\,, \\
(\eta_N^*, p) &= 0 \quad \forall p \in \mathcal{Z}_N\,,
\end{aligned} \tag{4}$$

and set $u_N^* = \eta_N^* + z_N^*$. We readily confirm the aforementioned background-update decomposition:

$$u_N^* = \eta_N^* + z_N^* = \Pi_{\mathcal{Z}_N^\perp} u^{\text{true}} + \Pi_{\mathcal{Z}_N} u^{\text{true}} = u^{\text{true}}.$$

We will primarily appeal to this saddle problem associated with the PBDW minimization statement to derive our data assimilation strategy and to develop associated theory.

2.3. Limited-observations statement

While the PBDW saddle statement (4) (or the minimization statement (1)) yields the exact state estimate $u_N^* = u^{\text{true}}$, the saddle statement is not actionable because the evaluation of (u^{true}, q) $\forall q \in \mathcal{U}$ in $(4)_1$ (or $(2)_2$) requires the full knowledge of the true state u^{true}. We wish to devise an actionable statement that approximates the solution using a finite number of observations.

Toward this end, we introduce observation functionals

$$\ell_m^o \in \mathcal{U}', \quad m = 1, \ldots, M_{\max},$$

DOI: 10.1002/nme

such that the m-th perfect experimental observation is modeled as $\ell_m^{\mathrm{o}}(u^{\mathrm{true}})$. In other words, the functionals model the particular transducer used in data acquisition. For instance, if the transducer measures a local state value, we may model the transducer by a Gaussian convolution

$$\ell_m^{\mathrm{o}}(v) = \mathrm{Gauss}(v; x_m^{\mathrm{c}}, r_m),$$

where x_m^{c} is the center of the Gaussian that reflects the transducer location and r_m is the standard deviation of the Gaussian that reflects the filter width of the transducer. We note that observation functionals can be quite general and in fact are only limited by the capabilities of the associated transducers. The set of functionals that are consistent with the experimentally realizable data acquisition procedures forms a library of observation functionals, denoted by $\mathscr{L}$. The library $\mathscr{L}$ may be finite or infinite; for instance, the library associated with Gaussian convolutions characterized by the observation center $x_m^{\mathrm{c}} \in \Omega \subset \mathbb{R}^d$, $\mathscr{L} = \{\ell \in \mathcal{U}' \mid \ell(\cdot) = \mathrm{Gauss}(\cdot; x_m^{\mathrm{c}}, r_m),\ x_m^{\mathrm{c}} \in \Omega\}$, is infinite dimensional. In general, observation functionals may be either more global or more localized; in this paper, we focus on 'pointwise' measurements, which we model—for experimental and mathematical reasons[§]—as local Gaussian convolutions. We in addition note that the precise form of the filter may not be important in cases for which the variation in the field occurs over scales much larger than r_m.

We then introduce, following Bennett [6], *experimentally observable* update spaces. Namely, we consider hierarchical spaces

$$\mathcal{U}_M = \mathrm{span}\{q_m \equiv R_{\mathcal{U}}\ell_m^{\mathrm{o}}\}_{m=1}^M, \quad M = 1, \ldots, M_{\max}, \ldots;$$

here again, the last ellipsis indicates that although in practice we shall consider M at most $M_{\max}$, in principle, we might extend the analysis to an infinite sequence of refinements. We recall that $R_{\mathcal{U}}\ell \in \mathcal{U}$ is the Riesz representation of $\ell \in \mathcal{U}'$. Then, for $q_m = R_{\mathcal{U}}\ell_m^{\mathrm{o}} \in \mathcal{U}_M$,

$$\big(u^{\mathrm{true}}, q_m\big) = \big(u^{\mathrm{true}}, R_{\mathcal{U}}\ell_m^{\mathrm{o}}\big) = \ell_m^{\mathrm{o}}(u^{\mathrm{true}})$$

is an experimental observation associated with the m-th transducer. It follows that, for any $q \in \mathcal{U}_M$, $(u^{\mathrm{true}}, q) = (u^{\mathrm{true}}, \sum_{m=1}^M \alpha_m q_m) = \sum_{m=1}^M \alpha_m \ell_m^{\mathrm{o}}(u^{\mathrm{true}})$; hence, (u^{true}, q) is a weighted sum of experimental observations. We say that $\mathcal{U}_M$ is *experimentally observable*.

We can now readily state our limited-observations PBDW minimization statement: find $(u_{N,M}^* \in \mathcal{U}, z_{N,M}^* \in \mathcal{Z}_N, \eta_{N,M}^* \in \mathcal{U})$ such that

$$\big(u_{N,M}^*, z_{N,M}^*, \eta_{N,M}^*\big) = \arg \inf_{\substack{u_{N,M} \in \mathcal{U} \\ z_{N,M} \in \mathcal{Z}_N \\ \eta_{N,M} \in \mathcal{U}}} \|\eta_{N,M}\|^2 \tag{5}$$

subject to

$$\begin{aligned} (u_{N,M}, v) &= (\eta_{N,M}, v) + (z_{N,M}, v) \quad \forall v \in \mathcal{U}, \\ (u_{N,M}, \phi) &= (u^{\mathrm{true}}, \phi) \quad \forall \phi \in \mathcal{U}_M. \end{aligned} \tag{6}$$

We arrive at the limited-observations minimization statement (5) from the unlimited-observations minimization statement (1) through a restriction of the test space for $(2)_2$ to $\mathcal{U}_M$. With this restriction, the right-hand side of $(6)_2$, $(u^{\mathrm{true}}, \phi)$ $\forall \phi \in \mathcal{U}_M$, is evaluated from the experimental observations.

We now derive (simplified) Euler–Lagrange equations associated with the limited-observations PBDW minimization statement (5). Following the construction for the unlimited-observations case, we first introduce the Lagrangian

$$\mathcal{L}(u_{N,M}, z_{N,M}, \eta_{N,M}, v, \phi_M) \equiv \frac{1}{2}\|\eta_{N,M}\|^2 + (u_{N,M} - \eta_{N,M} - z_{N,M}, v) + (u_{N,M} - u^{\mathrm{true}}, \phi_M);$$

[§]Mathematically, the pointwise value is in general ill-defined for functions in $\mathcal{U} \supset H_0^1(\Omega \subset \mathbb{R}^d)$, $d > 1$. Practically, any physical transducer has a finite filter width.

DOI: 10.1002/nme

here, $u_{N,M} \in \mathcal{U}$, $z_{N,M} \in \mathcal{Z}_N$, $\eta_{N,M} \in \mathcal{U}$, $v \in \mathcal{U}$, and $\phi_M \in \mathcal{U}_M$. We then obtain the (full) Euler–Lagrange equations: find $(u^*_{N,M} \in \mathcal{U}, z^*_{N,M} \in \mathcal{Z}_N, \eta^*_{N,M} \in \mathcal{U}, v^* \in \mathcal{U}, \phi^* \in \mathcal{U}_M)$ such that

$$\begin{aligned}
(v^*, \delta u) + (\phi^*, \delta u) &= 0 \quad \forall \delta u \in \mathcal{U}, \\
(v^*, \delta z) &= 0 \quad \forall \delta z \in \mathcal{Z}_N, \\
(\eta^*_{N,M}, \delta\eta) - (v^*, \delta\eta) &= 0 \quad \forall \delta\eta \in \mathcal{U}, \\
\left(u^*_{N,M} - \eta^*_{N,M} - z^*_{N,M}, \delta v\right) &= 0 \quad \forall \delta v \in \mathcal{U}, \\
\left(u^*_{N,M} - u^{\text{true}}, \delta\phi\right) &= 0 \quad \forall \delta\phi \in \mathcal{U}_M.
\end{aligned} \tag{7}$$

We now wish to simplify the statement. We first obtain from $(7)_1$ that $v^* = -\phi^*$; because $\phi^* \in \mathcal{U}_M$, we conclude that $v^* \in \mathcal{U}_M$. We then obtain from $(7)_3$ that $\eta^*_{N,M} = v^* = -\phi^*$; we again conclude that $\eta^*_{N,M} \in \mathcal{U}_M$. We now eliminate v^* (and ϕ^*) and rewrite $(7)_2$ as $(\eta^*_{N,M}, \delta z) = 0$ $\delta z \in \mathcal{Z}_N$. We next subtract $(7)_4$ from $(7)_5$ and test against $\mathcal{U}_M$ to obtain $(\eta^*_{N,M} + z^*_{N,M} - u^{\text{true}}, \delta v) = 0$ $\forall \delta v \in \mathcal{U}_M$. We hence obtain the simplified Euler–Lagrange equation associated with the PBDW minimization statement (5): find $(\eta^*_{N,M} \in \mathcal{U}_M, z^*_{N,M} \in \mathcal{Z}_N)$ such that

$$\begin{aligned}
(\eta^*_{N,M}, q) + (z^*_{N,M}, q) &= (u^{\text{true}}, q) \quad \forall q \in \mathcal{U}_M\ , \\
(\eta^*_{N,M}, p) &= 0 \quad \forall p \in \mathcal{Z}_N,
\end{aligned} \tag{8}$$

and set $u^*_{N,M} = \eta^*_{N,M} + z^*_{N,M}$.

Note that the limited-observations saddle was derived here from the limited-observations minimization statement (5); we may instead directly obtain the limited-observations saddle (8) from the unlimited-observations saddle (4) through a simple restriction of the trial space for the first variable and the test space for the first equation to the experimentally observable space $\mathcal{U}_M \subset \mathcal{U}$—the Galerkin recipe. We could also consider a Petrov–Galerkin approach in which $\eta^*_{N,M}$ is sought in a trial space informed by approximation requirements and different from the experimentally observable test space $\mathcal{U}_M$. Note that we may achieve a similar effect within the Galerkin context: we retain a single trial and test space for $\eta^*_{N,M}$ and the first equation of our saddle, respectively, and instead expand $\mathcal{Z}_N$ to include approximation properties beyond the best-knowledge model.

From (8), we readily observe that $\eta^*_{N,M} \in \mathcal{U}_M \cap \mathcal{Z}_N^\perp$ and $z^*_{N,M} \in \mathcal{Z}_N$. In words, because we wish to minimize $\|\eta^*_{N,M}\|$, $\eta^*_{N,M}$ should only accommodate the part of the projection onto $\mathcal{U}_M$, which cannot be absorbed by $z^*_{N,M} \in \mathcal{Z}_N$: the part that lies in $\mathcal{Z}_N^\perp$. In particular, we note that the first equation suggests the decomposition of the observable state $\Pi_{\mathcal{U}_M} u^{\text{true}}$ into two parts: $\Pi_{\mathcal{U}_M} u^{\text{true}} = \eta^*_{N,M} + \Pi_{\mathcal{U}_M} z^*_{N,M}$. In other words, the component $z^*_{N,M}$ is chosen such that its projection onto the observable space explains the observed data for a minimal $\eta^*_{N,M}$: $\Pi_{\mathcal{U}_M} z^*_{N,M} = \Pi_{\mathcal{U}_M} u^{\text{true}} - \eta^*_{N,M}$. The size of the saddle system is $M + N$.

We finally note that we may eliminate the variable $\eta^*_{N,M}$ from the saddle (8) and write the equation solely in terms of $z^*_{N,M}$: find $z^*_{N,M} \in \mathcal{Z}_N$ such that

$$\left(\Pi_{\mathcal{U}_M} z^*_{N,M}, v\right) = \left(\Pi_{\mathcal{U}_M} u^{\text{true}}, v\right) \quad \forall v \in \mathcal{Z}_N.$$

The Galerkin statement is associated with the minimization problem: find $z^*_{N,M} \in \mathcal{Z}_N$ such that $z^*_{N,M} = \arg\inf_{z \in \mathcal{Z}_N} \|\Pi_{\mathcal{U}_M}(u^{\text{true}} - z)\|$.

2.4. Algebraic form: offline–online computational decomposition

We consider an algebraic form of the PBDW state estimation problem (8). Toward this end, we first assume that elements of the infinite-dimensional space $\mathcal{U}$ are approximated in a suitably rich $\mathcal{N}$-dimensional approximation space; from hereon, in this section, all spaces are considered to be subspaces of this $\mathcal{N}$-dimensional approximation space. We introduce a hierarchical basis of (the $\mathcal{N}$-dimensional representation of) $\mathcal{Z}_{N_{\max}}$: $\{\zeta_n\}_{n=1}^{N_{\max}}$ such that $\mathcal{Z}_N = \text{span}\{\zeta_n\}_{n=1}^N$, $N = 1, \ldots, N_{\max}$. We similarly introduce a hierarchical basis of (the $\mathcal{N}$-dimensional representation of) $\mathcal{U}_{M_{\max}}$: $\{q_m\}_{m=1}^{M_{\max}}$ such that $\mathcal{U}_M = \text{span}\{q_m\}_{m=1}^M$, $M = 1, \ldots, M_{\max}$. Any element $z \in \mathcal{Z}_N$ may be expressed as

DOI: 10.1002/nme

$z = \sum_{n=1}^{N} \zeta_n \mathbf{z}_n$ for some $\mathbf{z} \in \mathbb{R}^N$; any element $\eta \in \mathcal{U}_M$ may be expressed as $\eta = \sum_{m=1}^{M} q_m \boldsymbol{\eta}_m$ for some $\boldsymbol{\eta} \in \mathbb{R}^M$.

In the offline stage, we then form matrices $\mathbf{A} \in \mathbb{R}^{M_{\max} \times M_{\max}}$ and $\mathbf{B} \in \mathbb{R}^{M_{\max} \times N_{\max}}$ such that

$$\begin{aligned} \mathbf{A}_{mm'} &= (q_{m'}, q_m), \quad m, m' = 1, \ldots, M_{\max}, \\ \mathbf{B}_{mn} &= (\zeta_n, q_m), \quad m = 1, \ldots, M_{\max},\ n = 1, \ldots, N_{\max}. \end{aligned}$$

If we wish to evaluate a functional output $\ell^{\text{out}}(u^*_{N,M})$, then we in addition form vectors $\mathbf{l}^{\text{out},U} \in \mathbb{R}^{M_{\max}}$ and $\mathbf{l}^{\text{out},Z} \in \mathbb{R}^{N_{\max}}$ such that

$$\begin{aligned} \left(\mathbf{l}^{\text{out},U}\right)_m &= \ell^{\text{out}}(q_m), \quad m = 1, \ldots, M_{\max}, \\ \left(\mathbf{l}^{\text{out},Z}\right)_n &= \ell^{\text{out}}(\zeta_n), \quad n = 1, \ldots, N_{\max}. \end{aligned}$$

The computation of the elements of $\mathcal{Z}_{N_{\max}}$ and $\mathcal{U}_{M_{\max}}$ and the formation of the matrices and vectors require $\mathcal{O}(\mathcal{N}^{\cdot})$ operations for some exponent that depends on the particular $\mathcal{Z}_N$ and $\mathcal{U}_M$ generation strategies.

In the online stage, we solve the algebraic form of (8): find $\boldsymbol{\eta}^* \in \mathbb{R}^M$ and $\mathbf{z}^* \in \mathbb{R}^N$ such that

$$\begin{pmatrix} \mathbf{A}_{1:M,1:M} & \mathbf{B}_{1:M,1:N} \\ \mathbf{B}^T_{1:M,1:N} & 0 \end{pmatrix} \begin{pmatrix} \boldsymbol{\eta}^* \\ \mathbf{z}^* \end{pmatrix} = \begin{pmatrix} \mathbf{l}^{\text{obs}} \\ 0 \end{pmatrix};$$

here, $\mathbf{A}_{1:M,1:M} \in \mathbb{R}^{M \times M}$ denotes the $M \times M$ principal submatrix of $\mathbf{A}$, $\mathbf{B}_{1:M,1:N} \in \mathbb{R}^{M \times N}$ denotes the $M \times N$ principal submatrix of $\mathbf{B}$, $(\cdot)^T$ denotes the transpose, and $\mathbf{l}^{\text{obs}} \in \mathbb{R}^M$ is the M-vector of experimentally observed values, $\mathbf{l}^{\text{obs}}_m = \ell^{\text{o}}_m(u^{\text{true}})$, $m = 1, \ldots, M$. The solution of the saddle system requires $\mathcal{O}((N+M)^3)$ operations.

Once the coefficients $\boldsymbol{\eta}^* \in \mathbb{R}^M$ and $\mathbf{z}^* \in \mathbb{R}^N$ are computed, we may find the field $u^*_{N,M}$ and the output $\ell^{\text{out}}(u^*_{N,M})$. Specifically, the state is given by $u^*_{N,M} = \eta^*_{N,M} + z^*_{N,M} = \sum_{m=1}^{M} q_m \boldsymbol{\eta}^*_m + \sum_{n=1}^{N} \zeta_n \mathbf{z}^*_n$; the evaluation requires $\mathcal{O}(\mathcal{N})$ operations. The output is given by $\ell^{\text{out}}(u^*_{N,M}) = \sum_{m=1}^{M} \mathbf{l}^{\text{out},U}_m \boldsymbol{\eta}^*_m + \sum_{n=1}^{N} \mathbf{l}^{\text{out},Z}_n \mathbf{z}^*_n$; the evaluation requires $\mathcal{O}(N+M)$ operations.

2.5. A priori error analysis

2.5.1. Field estimates. We appeal to the variational construction of the PBDW estimate and the existent theory on finite element analysis (e.g., [21]) to develop an *a priori* error theory for the PBDW formulation. We first state a proposition on the state (field) estimation error.

Proposition 2
The PBDW approximation error satisfies

$$\|\eta^*_N - \eta^*_{N,M}\| \leq \inf_{q \in \mathcal{U}_M \cap \mathcal{Z}_N^{\perp}} \inf_{z \in \mathcal{Z}_N} \|u^{\text{true}} - z - q\|,$$

$$\|z^*_N - z^*_{N,M}\| \leq \frac{1}{\beta_{N,M}} \inf_{q \in \mathcal{U}_M \cap \mathcal{Z}_N^{\perp}} \inf_{z \in \mathcal{Z}_N} \|u^{\text{true}} - z - q\|,$$

$$\|u^{\text{true}} - u^*_{N,M}\| \leq \left(1 + \frac{1}{\beta_{N,M}}\right) \inf_{q \in \mathcal{U}_M \cap \mathcal{Z}_N^{\perp}} \inf_{z \in \mathcal{Z}_N} \|u^{\text{true}} - z - q\|,$$

where the stability constant $\beta_{N,M}$ is defined by

$$\beta_{N,M} \equiv \inf_{z \in \mathcal{Z}_N} \sup_{q \in \mathcal{U}_M} \frac{(z,q)}{\|z\|\|q\|}.$$

DOI: 10.1002/nme

Proof
We subtract $(8)_1$ from $(4)_1$ and test against $q \in \mathcal{U}_M \cap \mathcal{Z}_N^\perp$ to obtain

$$\left(\eta_N^* - \eta_{N,M}^*, q\right) = 0 \quad \forall q \in \mathcal{U}_M \cap \mathcal{Z}_N^\perp.$$

It follows that, for any $q \in \mathcal{U}_M \cap \mathcal{Z}_N^\perp$,

$$\|\eta_N^* - \eta_{N,M}^*\|^2 = \left(\eta_N^* - \eta_{N,M}^*, \eta_N^* - q\right) + \left(\eta_N^* - \eta_{N,M}^*, q - \eta_{N,M}^*\right) \leqslant \|\eta_N^* - \eta_{N,M}^*\| \|\eta_N^* - q\|;$$

note that, in the last step, the second term vanishes: $(\eta_N^* - \eta_{N,M}^*, q - \eta_{N,M}^*) = 0$ because $q - \eta_{N,M}^* \in \mathcal{U}_M \cap \mathcal{Z}_N^\perp$. We thus obtain

$$\|\eta_N^* - \eta_{N,M}^*\| \leqslant \inf_{q \in \mathcal{U}_M \cap \mathcal{Z}_N^\perp} \|\eta_N^* - q\|.$$

Because $\eta_N^* = \Pi_{\mathcal{Z}_N^\perp} u^{\text{true}}$ and $q \in \mathcal{Z}_N^\perp$,

$$\begin{aligned}
\|\eta_N^* - \eta_{N,M}^*\|^2 &\leqslant \inf_{q \in \mathcal{U}_M \cap \mathcal{Z}_N^\perp} \|\Pi_{\mathcal{Z}_N^\perp} u^{\text{true}} - q\|^2 \\
&= \inf_{z \in \mathcal{Z}_N} \|\Pi_{\mathcal{Z}_N} u^{\text{true}} - z\|^2 + \inf_{q \in \mathcal{U}_M \cap \mathcal{Z}_N^\perp} \|\Pi_{\mathcal{Z}_N^\perp} u^{\text{true}} - q\|^2 \\
&= \inf_{q \in \mathcal{U}_M \cap \mathcal{Z}_N^\perp} \inf_{z \in \mathcal{Z}_N} \left(\|\Pi_{\mathcal{Z}_N} u^{\text{true}} - z\|^2 + \|\Pi_{\mathcal{Z}_N^\perp} u^{\text{true}} - q\|^2 \right) \\
&= \inf_{q \in \mathcal{U}_M \cap \mathcal{Z}_N^\perp} \inf_{z \in \mathcal{Z}_N} \|\Pi_{\mathcal{Z}_N} u^{\text{true}} - z + \Pi_{\mathcal{Z}_N^\perp} u^{\text{true}} - q\|^2 \\
&= \inf_{q \in \mathcal{U}_M \cap \mathcal{Z}_N^\perp} \inf_{z \in \mathcal{Z}_N} \|u^{\text{true}} - z - q\|^2.
\end{aligned}$$

Here, the first equality follows because $\inf_{z \in \mathcal{Z}_N} \|\Pi_{\mathcal{Z}_N} u^{\text{true}} - z\|^2 = 0$; the third equality follows from the Pythagorean theorem because $\Pi_{\mathcal{Z}_N} u^{\text{true}} - z \in \mathcal{Z}_N$ and $\Pi_{\mathcal{Z}_N^\perp} u^{\text{true}} - q \in \mathcal{Z}_N^\perp$. It follows that

$$\|\eta_N^* - \eta_{N,M}^*\| \leqslant \inf_{q \in \mathcal{U}_M \cap \mathcal{Z}_N^\perp} \inf_{z \in \mathcal{Z}_N} \|u^{\text{true}} - z - q\|, \tag{9}$$

which is the bound on $\|\eta_N^* - \eta_{N,M}^*\|$.

We next subtract $(8)_1$ from $(4)_1$ and test against $q \in \mathcal{U}_M$ to obtain

$$\left(\eta_N^* - \eta_{N,M}^*, q\right) + \left(z_N^* - z_{N,M}^*, q\right) = 0 \quad \forall q \in \mathcal{U}_M.$$

It follows from $z_N^* - z_{N,M}^* \in \mathcal{Z}_N$ and the definition of the inf-sup constant that

$$\beta_{N,M} \|z_N^* - z_{N,M}^*\| \leqslant \sup_{v \in \mathcal{U}_M} \frac{\left(z_N^* - z_{N,M}^*, v\right)}{\|v\|} = \sup_{v \in \mathcal{U}_M} \frac{-\left(\eta_N^* - \eta_{N,M}^*, v\right)}{\|v\|} \leqslant \|\eta_N^* - \eta_{N,M}^*\|.$$

Combined with (9), we obtain

$$\|z_N^* - z_{N,M}^*\| \leqslant \frac{1}{\beta_{N,M}} \inf_{q \in \mathcal{U}_M \cap \mathcal{Z}_N^\perp} \inf_{z \in \mathcal{Z}_N} \|u^{\text{true}} - z - q\|,$$

which is the bound on $\|z_N^* - z_{N,M}^*\|$.

DOI: 10.1002/nme

We finally invoke the triangle inequality,

$$\|u^{\text{true}} - u^*_{N,M}\| \leq \|\eta^*_N - \eta^*_{N,M}\| + \|z^*_N - z^*_{N,M}\| \leq \left(1 + \frac{1}{\beta_{N,M}}\right) \inf_{q \in \mathcal{U}_M \cap \mathcal{Z}_N^\perp} \inf_{z \in \mathcal{Z}_N} \|u^{\text{true}} - z - q\|,$$

which is the bound on $\|u^{\text{true}} - u^*_{N,M}\|$. □

Proposition 2 identifies three distinct contributions to the error in the field estimate. First is the stability constant, $\beta_{N,M}$; the better the stability, the smaller the error. Second is the background best-fit error, $\inf_{z \in \mathcal{Z}_N} \|u^{\text{true}} - z\|$; the error is small if u^{true} is well approximated in the background space $\mathcal{Z}_N$. Third is the update best-fit error, $\inf_{q \in \mathcal{U}_M \cap \mathcal{Z}_N^\perp} \|\Pi_{\mathcal{Z}_N^\perp} u^{\text{true}} - q\|$; the components of u^{true} that do not lie in $\mathcal{Z}_N$ are treated by the update space. We will appeal in Section 2.7 to these observations to select $\mathcal{Z}_N$ and $\mathcal{U}_M$.

2.5.2. Output estimates. We may also develop an *a priori* error bound associated with an estimate of a functional output.

Proposition 3
Let $\ell^{\text{out}} \in \mathcal{U}'$ be the output functional of interest, and define $\psi = R_{\mathcal{U}} \ell^{\text{out}} \in \mathcal{U}$ as the adjoint associated with the output. The output error satisfies

$$\begin{aligned} |\ell^{\text{out}}(u^{\text{true}}) - \ell^{\text{out}}(u^*_{N,M})| &= |\left(u^{\text{true}} - u^*_{N,M}, \psi - \Pi_{\mathcal{U}_M} \psi\right)| \\ &\leq \|u^{\text{true}} - u^*_{N,M}\| \|\psi - \Pi_{\mathcal{U}_M} \psi\|. \end{aligned}$$

Proof
We first note that

$$\ell^{\text{out}}(w) = \left(R_{\mathcal{U}} \ell^{\text{out}}, w\right) = (\psi, w) \quad \forall w \in \mathcal{U}$$

by the definition of the Riesz operator and the adjoint ψ. We next note that, by Galerkin orthogonality, $(u^{\text{true}} - u^*_{N,M}, q) = 0 \; \forall q \in \mathcal{U}_M$. It follows that

$$|\ell^{\text{out}}\left(u^{\text{true}} - u^*_{N,M}\right)| = |\left(u^{\text{true}} - u^*_{N,M}, \psi\right)| = |\left(u^{\text{true}} - u^*_{N,M}, \psi - \Pi_{\mathcal{U}_M} \psi\right)|.$$

We finally invoke Cauchy–Schwarz to obtain the desired bound. □

Proposition 3 suggests that the error in a functional output depends on, in addition to the factors that affect the field estimate, the approximation of the adjoint by the update space. Similar to the finite element approximation, we expect the output estimate to 'superconverge' with M, as both the approximation of the primal and adjoint states contributes to the reduction in the output error.

2.5.3. Stabilization. Proposition 2 shows that the stability constant $\beta_{N,M}$ plays a key role in controlling the state estimation error. As regards its behavior, we have the following proposition.

Proposition 4
The inf-sup constant

$$\beta_{N,M} \equiv \inf_{z \in \mathcal{Z}_N} \sup_{q \in \mathcal{U}_M} \frac{(z, q)}{\|z\| \|q\|}$$

is a non-increasing function of the dimension of the background space, N, and a non-decreasing function of the dimension of the observable space, M. Furthermore, $\beta_{N,M} = 0$ for $M < N$.

Proof
The result is a direct consequence of the expansion of the infimizer space $\mathcal{Z}_N$ and the supremizer space $\mathcal{U}_M$. □

DOI: 10.1002/nme

2.5.4. Approximation properties of $\mathcal{U}_M$ for pointwise measurements in one dimension. Proposition 2 suggests that the update space $\mathcal{U}_M$ plays a role in estimating the component of state that lies in $\mathcal{Z}_N^\perp$. We hence wish to quantify the approximation properties of the space $\mathcal{U}_M$. We do not have a characterization of the approximation properties for a general physical dimension d, inner product $(\cdot,\cdot)$, and output functional $\ell_m^o(\cdot)$; we can however quantify the approximation properties in a very specialized case.

Proposition 5
We introduce a domain $\Omega \equiv]0,1[$ and a space $\mathcal{U} \equiv H_0^1(\Omega)$ equipped with an inner product $(w,v) \equiv \int_\Omega \frac{\partial w}{\partial x}\frac{\partial v}{\partial x}dx$ and the associated induced norm $|\cdot|_{H^1(\Omega)}$. Let $u^{\text{true}} \in H_0^1(\Omega) \cap H^2(\Omega)$. Consider pointwise observation functionals $\ell_m^o \equiv \delta(\cdot, x_m^o)$, $m = 1,\ldots,M$, with uniformly spaced centers $\{x_m^o\}_{m=1}^M$; here, δ denotes the Dirac delta. We denote the associated update space by $\mathcal{U}_M \equiv \text{span}\{R_\mathcal{U}\ell_m^o\}_{m=1}^M$. Then, the update best-fit error is bounded by

$$\inf_{q\in\mathcal{U}_M} \|u^{\text{true}} - q\|_{H^r(\Omega)} \leqslant CM^{-(2-r)}\|u^{\text{true}}\|_{H^2(\Omega)}$$

for $r = 0, 1$ and some C independent of M and u^{true}.

Proof
Because $u^{\text{true}} \in H_0^1(\Omega) \cap H^2(\Omega)$ and $\|\cdot\| = |\cdot|_{H^1(\Omega)}$, it suffices to show that $\mathcal{U}_M$ is a space of piecewise linear polynomials,

$$\mathcal{X}_M \equiv \{w \in C^0(\Omega) \mid w|_{I_k} \in \mathbb{P}^1(I_k), k = 1,\ldots,M+1\},$$

for $I_1 = [0, x_1]$, $I_{M+1} = [x_M, 1]$, and $I_k = [x_k, x_{k+1}]$, $k = 2,\ldots,M-1$. (Without loss of generality, we assume $0 \leqslant x_1 < \cdots < x_M \leqslant 1$.) Toward this end, we first note that for $\ell_m^o = \delta(\cdot, x_m^o)$ and $\|\cdot\| = |\cdot|_{H^1(\Omega)}$, a function $R_\mathcal{U}\ell_m^o \in \mathcal{U}$ is the piecewise linear 'hat' function with the peak (or the derivative jump) at x_m^o; in particular, $R_\mathcal{U}\ell_m^o \in \mathcal{U}_M$. We then note that the functions $\{R_\mathcal{U}\ell_m^o\}_{m=1}^M$ are linearly independent because x_m^o (and hence the location of the derivative jumps) are different. We thus have M linearly independent functions in the M-dimensional space $\mathcal{U}_M$; thus, $\{R_\mathcal{U}\ell_m^o\}_{m=1}^M$ is a basis for $\mathcal{U}_M$, and in particular, $\mathcal{U}_M \equiv \text{span}\{R_\mathcal{U}\ell_m^o\}_{m=1}^M = \mathcal{X}_M$. This concludes the proof. □

On one hand, Proposition 5 shows that we can expect the update best-fit error to decrease with M, and hence, combined with Proposition 2, $u_{N,M}^*$ converges to u^{true} in the limit of $M \to \infty$. On the other hand, Proposition 5 shows that the convergence of the error with the number of observations M is rather slow: the $H^1(\Omega)$ and $L^2(\Omega)$ errors converge as M^{-1} and M^{-2}, respectively, in one dimension. More generally, we expect the $H^1(\Omega)$ and $L^2(\Omega)$ errors to converge as $M^{-1/d}$ and $M^{-2/d}$, respectively, in a d-dimensional space. In order to obtain a good estimate with a reasonable number of observations M, we must choose the background space $\mathcal{Z}_N$ appropriately such that the update $\eta_N^* \in \Pi_{\mathcal{Z}_N^\perp} u^{\text{true}}$ is small.

2.6. A posteriori error estimates

We introduce an *a posteriori* error estimate for the state estimate $u_{N,M}^*$,

$$E_{N,M,M'} \equiv \|u_{N,M'}^* - u_{N,M}^*\|,$$

where M', such that $M \leqslant M' \leqslant M_{\max}$, is the number of observations used to form the error estimate. We similarly introduce an *a posteriori* error estimate for the output estimate $\ell^{\text{out}}(u_{N,M}^*)$,

$$O_{N,M,M'} \equiv |\ell^{\text{out}}\left(u_{N,M'}^*\right) - \ell^{\text{out}}\left(u_{N,M}^*\right)|,$$

again based on $M' \geqslant M$ observations. We note that, for $M' = M$, $E_{N,M,M'} = 0$ and $O_{N,M,M'} = 0$.

DOI: 10.1002/nme

Remark 1
The field *a posteriori* error estimate $E_{N,M,M'}$ may be interpreted as an approximation of the (dual) norm of the error $u^{\text{true}} - u^*_{N,M}$ using the M'-dimensional subspace $\mathcal{U}_{M'} \subset \mathcal{U}$ as the test space:

$$E_{N,M,M'} = \sup_{q \in \mathcal{U}_{M'}} \frac{|(u^{\text{true}}, q) - (u^*_{N,M}, q)|}{\|q\|}.$$

The equivalence follows from $(u^*_{N,M'}, q) = (u^{\text{true}}, q)\ \forall q \in \mathcal{U}_{M'}$. Assuming $\mathcal{U}_{M'} \to \mathcal{U}$ as $M' \to \infty$, the (dual) norm estimate converges to the true (dual) norm of the error.

2.7. Construction of spaces: offline

2.7.1. Best-knowledge model. As we have just described, Proposition 2 suggests that we should choose the background space $\mathcal{Z}_N$ such that the background best-fit error $\inf_{z \in \mathcal{Z}_N} \|u^{\text{true}} - z\|$ is small. We consider a parametric construction of the spaces $\mathcal{Z}_N$, $N = 1, \ldots, N_{\max}$, such that the background best-fit error decreases rapidly with N.

Toward this end, we now formally introduce the parameterized best-knowledge model previously discussed in the introduction. We first introduce a parameter $\mu \in \mathcal{D}$; here, $\mathcal{D} \subset \mathbb{R}^P$ is the parameter domain associated with the anticipated, or parametric, uncertainty in the best-knowledge model. We next introduce a parameterized form: $G^\mu : \mathcal{U} \times \mathcal{U} \to \mathbb{R}$; we assume that the form is linear in the second argument. We then define, for a given $\mu \in \mathcal{D}$, the best-knowledge solution $u^{\text{bk},\mu} \in \mathcal{U}$ that satisfies

$$G^\mu(u^{\text{bk},\mu}, v) = 0 \quad \forall v \in \mathcal{U};$$

we assume that the problem is well posed; that is, for any $\mu \in \mathcal{D}$, $u^{\text{bk},\mu}$ exists and is unique. We now introduce the best-knowledge parameterized manifold

$$\mathcal{M}^{\text{bk}} \equiv \{u^{\text{bk},\mu} \mid \mu \in \mathcal{D}\}.$$

We intend to choose the parameterized form G^μ and the parameter domain $\mathcal{D}$ to minimize the model error

$$\epsilon^{\text{bk}}_{\text{mod}}(u^{\text{true}}) \equiv \inf_{w \in \mathcal{M}^{\text{bk}}} \|u^{\text{true}} - w\| = \|u^{\text{true}} - F_{\mathcal{M}^{\text{bk}}} u^{\text{true}}\|,$$

where $F_{\mathcal{M}^{\text{bk}}} u^{\text{true}} \in \mathcal{M}^{\text{bk}}$ is an infimizer.

2.7.2. Background spaces $\mathcal{Z}_N$. As mentioned in the introduction, we condense the best-knowledge of $\mathcal{M}^{\text{bk}}$ into an N-dimensional linear space $\mathcal{Z}_N$ through several different model-reduction processes: $\textsc{Process}^{\mathcal{Z}}_N(\mathcal{M}^{\text{bk}}) \to \mathcal{Z}_N$. Here, we list a few:

- POD: $\textsc{Process}^{\mathcal{Z}}_N \equiv \textbf{POD}_N$.
  We first introduce a training set $\Xi_{\text{train}} \subset \mathcal{D}$ that sufficiently covers the parameter domain $\mathcal{D}$. We then evaluate the best-knowledge solution at each training point to form the set $\{u^{\text{bk},\mu}\}_{\mu \in \Xi_{\text{train}}}$. We finally apply POD [7] to $\{u^{\text{bk},\mu}\}_{\mu \in \Xi_{\text{train}}}$ and extract the N most dominant modes as measured in $\|\cdot\|$ to form $\mathcal{Z}_N$.
- Weak greedy: $\textsc{Process}^{\mathcal{Z}}_N \equiv \textbf{WeakGreedy}_N$.
  We apply the weak greedy algorithm described in Algorithm 1 to form $\mathcal{Z}_N$ (see also a detailed review—in particular, as regards the construction of an error bound that is efficient in the many-query setting—by Rozza *et al.* [3]). The algorithm has been proven to generate an optimal sequence of spaces with respect to the Kolmogorov width of $\mathcal{M}^{\text{bk}}$ in [5, 25, 26]. We emphasize that even if the best-knowledge model is effectively exact, typically, we cannot apply the standard reduced basis Galerkin approach in the online stage because we anticipate that in

DOI: 10.1002/nme

many situations, the parameter values of some particular configuration will not be known precisely; hence, we incorporate only the offline of the reduced basis framework, in particular in the development of $\mathcal{Z}_N$.

- Taylor expansion: $\textsc{Process}_N^{\mathcal{Z}} \equiv \textsc{Taylor}_N^{\mu_0}$. We first evaluate the parametric derivatives of the solution $u^{\text{bk},\mu}$: $\zeta_p = [\partial u^{\text{bk},\mu}/\partial \mu_p]_{\mu=\mu_0}$, $p = 1, \ldots, P$. We then form $\mathcal{Z}_{N=P} = \text{span}\{\zeta_p\}_{p=1}^P$. We may also consider higher-order expansions [8].
  We may in addition consider other model order reduction approaches, such as the proper generalized decomposition [27].

Algorithm 1: WeakGreedy$_M$ algorithm

input : G^μ: parameterized best-knowledge model
$\mathcal{D}$: parameter domain
$\Delta_N^{\text{bk},\mu}$: error estimate for $\inf_{z\in\mathcal{Z}_N} \|u^{\text{bk},\mu} - z\| \leqslant \Delta_N^{\text{bk},\mu}$
output: $\{\mathcal{Z}_N\}_{N=1}^{N_{\max}}$: sequence of $N_{\max}$ hierarchical background spaces

1 for $M = 1, \ldots, N_{max}$ **do**
2 Identify the parameter associated with the largest error estimate

$$\tilde{\mu}_N = \arg \sup_{\mu\in\Xi_{\text{train}}\in\mathcal{D}} \Delta_{N-1}^{\text{bk},\mu}$$

3 Evaluate the associated solution

$$\zeta_N = u^{\text{bk},\tilde{\mu}_N}$$

4 Augment the background space

$$\mathcal{Z}_N = \text{span}\{\mathcal{Z}_{N-1}, \zeta_N\}$$

5 end

In general, we may quantify the approximation property of the background space in terms of the best-fit error

$$\epsilon_N^{\text{bk}}(u^{\text{true}}) \equiv \inf_{w\in\mathcal{Z}_N} \|u^{\text{true}} - w\|.$$

In particular, if the space $\mathcal{Z}_N$ is generated from the best-knowledge manifold $\mathcal{M}^{\text{bk}}$, we may decompose the error into two parts and identify two different sources of the error:

$$\begin{aligned}
\epsilon_N^{\text{bk}}(u^{\text{true}}) &\equiv \inf_{w\in\mathcal{Z}_N} \|u^{\text{true}} - w\| \leqslant \|u^{\text{true}} - \Pi_{\mathcal{Z}_N} F_{\mathcal{M}^{\text{bk}}}(u^{\text{true}})\| \\
&\leqslant \|u^{\text{true}} - F_{\mathcal{M}^{\text{bk}}}(u^{\text{true}})\| + \|F_{\mathcal{M}^{\text{bk}}}(u^{\text{true}}) - \Pi_{\mathcal{Z}_N} F_{\mathcal{M}^{\text{bk}}}(u^{\text{true}})\| \\
&\leqslant \inf_{w\in\mathcal{M}^{\text{bk}}} \|u^{\text{true}} - w\| + \sup_{w\in\mathcal{M}^{\text{bk}}} \|w - \Pi_{\mathcal{Z}_N} w\| \\
&\leqslant \epsilon_{\text{mod}}^{\text{bk}}(u^{\text{true}}) + \epsilon_{\text{disc},N}^{\text{bk}}.
\end{aligned}$$

The first term, $\epsilon_{\text{mod}}^{\text{bk}}(u^{\text{true}}) \equiv \inf_{w\in\mathcal{M}^{\text{bk}}} \|u^{\text{true}} - w\|$, is the *modeling error*, which arises from the fact that we cannot in general anticipate all forms of uncertainty and provide the associated parameterized model; hence, in general, $u^{\text{true}} \notin \mathcal{M}^{\text{bk}}$, and $\epsilon_{\text{mod}}^{\text{bk}}(u^{\text{true}}) \neq 0$. The second term, $\epsilon_{\text{disc},N}^{\text{bk}} \equiv \sup_{w\in\mathcal{M}^{\text{bk}}} \|w - \Pi_{\mathcal{Z}_N} w\|$, is the *discretization error*, which arises from the fact that we cannot in general construct an N-dimensional linear space that can represent all elements of $\mathcal{M}^{\text{bk}}$; hence, in general, $\mathcal{M}^{\text{bk}} \not\subset \mathcal{Z}_N$, and $\epsilon_{\text{disc},N}^{\text{bk}} \neq 0$. For some constructions of $\mathcal{Z}_N$, we may rigorously

DOI: 10.1002/nme

bound the *discretization* error; for example, in the weak greedy procedure with error bounds, $\epsilon^{\text{bk}}_{\text{disc},N} \leq \Delta^{\text{bk},\mu}_N$. On the other hand, we cannot in general bound the *modeling* error.

2.7.3. Superdomains for the best-knowledge model. As mentioned in the introduction, projection-by-data, unlike projection-by-model, does not require boundary conditions (and initial conditions). However, in order to obtain best-knowledge solutions and to construct $\mathcal{Z}_N$, the best-knowledge model must be defined on a domain on which the boundary-value problem is well posed. Hence, in general, the domain on which we wish to estimate the state, $\Omega \subset \mathbb{R}^d$, may differ from the domain associated with the best-knowledge model, $\Omega^{\text{bk}} \supset \Omega$. More generally, the domain Ω may be a manifold in Ω^{bk}: $\Omega^{\text{bk}} \subset \mathbb{R}^{d'}$ for $d' > d$.

In this generalized setting, to construct $\mathcal{Z}_N$, we first identify the Hilbert space associated with Ω^{bk} by $\mathcal{U}^{\text{bk}} = \mathcal{U}^{\text{bk}}(\Omega^{\text{bk}})$. We then identify the best-knowledge manifold, $\mathcal{M}^{\text{bk}} \equiv \{u^{\text{bk},\mu} \in \mathcal{U}^{\text{bk}} \mid \mu \in \mathcal{D}\}$. We next construct the background space on Ω^{bk}, $\textsc{Process}^{\mathcal{Z}}_N(\mathcal{M}^{\text{bk}}) \rightarrow \mathcal{Z}^{\text{bk}}_N$. We finally form the background space on Ω, $\mathcal{Z}_N = \{z \in \mathcal{U} \mid z = z^{\text{bk}}|_\Omega,\ z^{\text{bk}} \in \mathcal{Z}^{\text{bk}}_N\}$.[¶] The procedure allows us to focus on data assimilation on $\Omega \subset \Omega^{\text{bk}}$ even if the best-knowledge model is only well posed on $\Omega^{\text{bk}} \supset \Omega$.

2.7.4. Experimentally observable update spaces $\mathcal{U}_M$: design of experiment. Proposition 2 shows that, for a given $\mathcal{Z}_N$, the selection of the experimentally observable update spaces $\mathcal{U}_M$ should be based on two criteria:

- The maximization of the stability constant $\beta_{N,M} = \inf_{w \in \mathcal{Z}_N} \sup_{v \in \mathcal{U}_M} (w, v)/(\|w\|\|v\|)$; to improve stability, we wish to choose $\mathcal{U}_M$ such that any element in $\mathcal{Z}_N$ is well approximated by an element in $\mathcal{U}_M$.
- The minimization of the approximation error $\inf_{\eta \in \mathcal{U}_M \cap \mathcal{Z}_N^\perp} \|\Pi_{\mathcal{Z}_N^\perp} u^{\text{true}} - \eta\|$ (and in particular the modeling error $\inf_{w \in \mathcal{M}^{\text{bk}}} \|u^{\text{true}} - w\|$); to improve approximation, we wish to choose $\mathcal{U}_M$ such that elements in $\mathcal{Z}_N^\perp$—that is, elements outside of $\mathcal{Z}_N$—are well approximated by $\mathcal{U}_M$.

We emphasize that $\mathcal{U}_M$ must be experimentally observable: $\mathcal{U}_M = \text{span}\{q_m \equiv R_{\mathcal{U}} \ell^{\text{o}}_m\}^M_{m=1}$, $M = 1, \ldots, M_{\max}$. Note that, by construction, the experimentally observable space is a function of the choice of the inner product $(\cdot, \cdot)$.

We recall that in general the PBDW framework accommodates a library $\mathscr{L}$ that consists of candidate observation functionals that are consistent with an experimentally realizable data acquisition procedure. In this paper, however, we focus on localized observations using a given transducer, $\ell^{\text{o}}_m(\cdot) = \text{Gauss}(\cdot; x^{\text{c}}_m, r_m)$, whose location of the centers $\{x^{\text{c}}_m\}^M_{m=1}$ largely determines the space $\mathcal{U}_M$. We may select the observation functionals from $\mathscr{L}$ (and more specifically the observation centers) using several different processes: $\textsc{Process}^{\mathcal{U}}_M(\mathcal{Z}_{N_{\max}}) \rightarrow \mathcal{U}_M$. Here, we list a few (some of which are specialized for localized observations):

- Quasi-uniform or random: $\textsc{Process}^{\mathcal{U}}_M \equiv \textsc{QuasiUniform}_M$ or $\textsc{RandomUniform}_M$.
  This procedure is specialized to localized observations. The algorithm aims to minimize the approximation error by providing a uniform coverage of the domain. $\textsc{QuasiUniform}_M$ is a deterministic sequential procedure: at step m, we insert a new point at the location that maximizes the shortest distance to the set of points at step $m-1$. $\textsc{RandomUniform}_M$ is a stochastic sequential procedure: we simply draw points sequentially from the uniform density over Ω.
- GEIM [10, 28]: $\textsc{Process}^{\mathcal{U}}_M \equiv \texttt{GEIM}_M$.
  We select, in a greedy manner from $\mathscr{L}$, a sequence of observation functionals aimed to minimize the interpolation error associated with the approximation space $\mathcal{Z}_{N_{\max}} \subset \mathcal{U}$. The algorithm works for $M = N$, $N = 1, \ldots, N_{\max}$.
- Greedy stability maximization: $\textsc{Process}^{\mathcal{U}}_M \equiv \textsc{SGreedy}_M$.
  The procedure is described in Algorithm 2. In short, the algorithm chooses a sequence of

[¶]The restriction of the basis of $\mathcal{Z}^{\text{bk}}_N$ to the domain $\Omega \subset \Omega^{\text{bk}}$ may yield an ill-conditioned basis. To reinforce the robustness of the approach, one could extract, from the ill-conditioned basis of cardinality N, a subset of cardinality $N' < N$ based on, for instance, a singular-value decomposition.

DOI: 10.1002/nme

observation functionals from a library $\mathscr{L}$ to maximize the inf-sup constant $\beta_{N,M}$ in a greedy manner. Unlike the preceding $\texttt{GEIM}_M$ algorithm, the $\texttt{SGREEDY}_M$ algorithm is applicable for $M > N$. The $\texttt{SGREEDY}_M$ algorithm is equivalent to $\texttt{GEIM}_M$ for $M = N$.

- Greedy stability maximization (for localized observations): $\texttt{PROCESS}_M^{\mathcal{U}} \equiv \texttt{SGREEDY}_M^{\text{local}}$.
  This is a derivative of the $\texttt{SGREEDY}_M$ algorithm for localized observation functionals, that is, $\mathscr{L} = \{\ell \in \mathcal{U}' \mid \ell(\cdot) = \text{Gauss}(\cdot; x_m^{\text{c}}, r_m),\ x_m^{\text{c}} \in \Omega\}$. In this procedure, step 5 of the $\texttt{SGREEDY}_M$ algorithm described in Algorithm 2 is approximated by a two-step procedure: the identification of the least well-approximated point $\tilde{x} = \arg\sup_{x\in\Omega} |(w_{\text{inf}} - v_{\text{sup}})(x)|$ and the construction of $\ell_M^{\text{o}} = \text{Gauss}(\cdot; \tilde{x}, r_M)$. For a sufficiently small filter width r_m, the approximation gives a reasonable and convenient estimate of the 'proper' $\texttt{SGREEDY}_M$ algorithm. We assume that members of $\mathcal{Z}_N$ are sufficiently regular to justify pointwise evaluation.
- Greedy stability–approximation balancing [23]: $\texttt{PROCESS}_M^{\mathcal{U}} \equiv \texttt{SAGREEDY}$.
  The algorithm is a combination of the preceding $\texttt{SGREEDY}_M$ and $\texttt{RANDOMUNIFORM}_M$ algorithms. We initially invoke the $\texttt{SGREEDY}_M$ algorithm to maximize the stability until a user-specified threshold stability constant is achieved for $N = N_{\max}$. We then invoke $\texttt{RANDOMUNIFORM}_M$ sampling to minimize the approximation error; this second step is specialized to localized observations. Note that, because the stability constant is a non-decreasing function of M for a fixed N, the stability constant remains above the threshold in the second stage.
  We will see in the results section that the stability-maximization algorithm provides a more stable estimate of the state than a set of random points, especially when M is close to N.

Algorithm 2: $\texttt{SGREEDY}_M$ stability-maximization algorithm

input : $\{\mathcal{Z}_N\}_{N=1}^{N_{\max}}$: background approximation spaces
$\mathscr{L}$: a library of candidate observation functionals
output: $\{\ell_m^{\text{o}}\}_{m=1}^{M_{\max}}$: observation functionals
$\{\mathcal{U}_M\}_{M=1}^{M_{\max}}$: experimentally observable update spaces

for $M = 1, \ldots, M_{max}$ **do** // construct $\mathcal{U}_M$ given $\mathcal{U}_{M-1}$

Set $N = \min\{N_{\max}, M\}$.

Compute the least-stable mode: for $M > 1$,

$$w_{\text{inf}} = \arg \inf_{w\in\mathcal{Z}_N} \sup_{v\in\mathcal{U}_{M-1}} \frac{(w, v)}{\|w\|\|v\|};$$

for $M = 1$, set w_{inf} to a normalized basis for $\mathcal{Z}_{N=M=1}$.

Compute the associated supremizer

$$v_{\text{sup}} = \Pi_{\mathcal{U}_{M-1}} w_{\text{inf}}.$$

Identify the least well-approximated functional

$$\ell_M^{\text{o}} = \arg \sup_{\ell\in\mathscr{L}} |\ell(w_{\text{inf}} - v_{\text{sup}})|$$

Set

$$\mathcal{U}_M = \text{span}\{\mathcal{U}_{M-1}, R_{\mathcal{U}}\ell_M^{\text{o}}\}.$$

end

Per Proposition 4, for $M < N$, the inf-sup constant is zero. Thus, we may not consider $M < N$. However, there is nevertheless a 'few-sample' regime, or at least a circumstance that will result in relatively small M: if the modeling error is small and the model-reduction process is efficient such that N is small, then typically (say with the $\texttt{SGREEDY}_M$ algorithm), we may chose M small.

DOI: 10.1002/nme

This few-observations regime is important in particular because often—and in our example of Section 4—it is the observations that dominate the online cost.

3. SYNTHETIC PROBLEM: HELMHOLTZ IN $\mathbb{R}^2$

3.1. Model form

We study the behavior of the PBDW formulation using a two-dimensional Helmholtz problem. Toward this end, we consider a complex extension of the PBDW formulation presented in Section 2. We first introduce a domain $\Omega \equiv]0,1[^2$ and the Hilbert space $\mathcal{U} \equiv H^1(\Omega)$ endowed with the standard H^1 inner product and norm:

$$(w,v) \equiv \int_\Omega (\nabla w \cdot \nabla \bar{v} + w\bar{v})dx \quad \text{and} \quad \|w\| \equiv \sqrt{(w,w)}.$$

We then consider the following weak statement: find $\Upsilon_g^\mu \in \mathcal{U}$ such that

$$a^\mu(\Upsilon_g^\mu, v) = f_g^\mu(v) \quad \forall v \in \mathcal{U},$$

where

$$a^\mu(w,v) \equiv (1+i\epsilon\mu)\int_\Omega \nabla w \cdot \nabla \bar{v} dx - \mu^2 \int_\Omega w\bar{v}dx \quad \forall w,v \in \mathcal{U},$$

$$f_g^\mu(v) \equiv \mu \int_\Omega \left(2x_1^2 + \exp(x_2)\right)\bar{v}dx + \mu\int_\Omega g\bar{v}dx \quad \forall v \in \mathcal{U},$$

for a parameter (i.e., the wavenumber) $\mu \in \mathbb{R}_{>0}$, a function $g \in L^2(\Omega)$, and a fixed dissipation $\epsilon = 10^{-3}$. Note that $\bar{(\cdot)}$ denotes the complex conjugate of $(\cdot)$. Here, the wavenumber μ constitutes the anticipated, and parametric, uncertainty—the term might model for instance the uncertainty in the speed of sound; the function g constitutes the unanticipated, and nonparametric, uncertainty—the term accommodates all other sources of uncertainty. We also consider a functional output:

$$\ell^{\text{out}}(w) \equiv \int_{\Gamma_1} w ds,$$

where $\Gamma_1 \equiv \{(x_1,x_2) \in \mathbb{R}^2 |\ x_1 = 0,\ x_2 \in]0,1[\}$. We approximate the solution in a $8 \times 8 \times 2$ (128-element) triangular $\mathbb{P}^5$ finite element space, $\mathcal{U}^{\mathcal{N}} \subset \mathcal{U}$.

3.2. Synthetic truths

To assess the performance of the PBDW formulation for various configurations, we consider a number of 'test truths' associated with different wavenumbers and two choices of the bias function g. The truth wavenumber $\tilde{\mu}$ takes on a value in the interval $[2,10]$. The two bias functions $\tilde{g}$ are given by

$$\tilde{g} = \begin{cases} \tilde{g}_{\text{I}} \equiv 0, & \text{case I} \\ \tilde{g}_{\text{II}} \equiv 0.5(\exp(-x_1) + \cos(1.3\pi x_2)), & \text{case II.} \end{cases}$$

A given truth is defined by a particular truth parameter $\tilde{\mu}$ and bias $\tilde{g}$: $u^{\text{true}} \equiv \Upsilon_{\tilde{g}}^{\tilde{\mu}}$. We show in Figure 1(a–c) the truth fields for case I for a few different combinations of wavenumbers and biases. We also show in Figure 1(d) the variation in $\|u^{\text{true}}\|$ as a function of the wavenumber $\tilde{\mu}$; note that there are three resonances in the parameter range considered.

DOI: 10.1002/nme

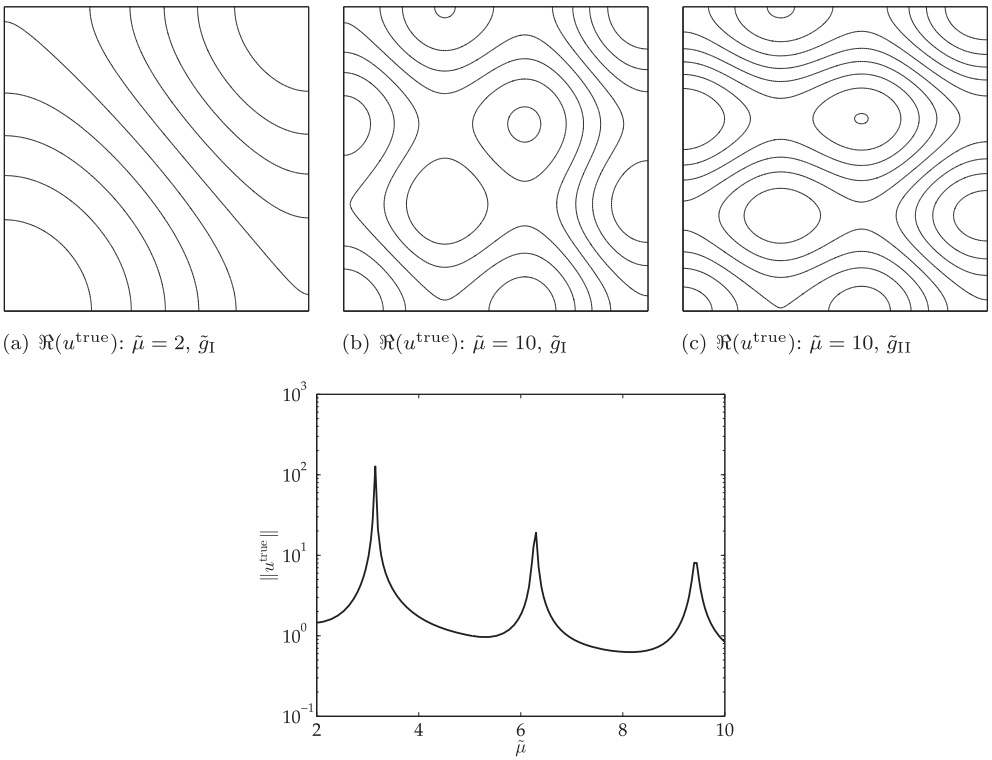

(a) $\Re(u^{\text{true}})$: $\tilde{\mu} = 2$, $\tilde{g}_{\text{I}}$ (b) $\Re(u^{\text{true}})$: $\tilde{\mu} = 10$, $\tilde{g}_{\text{I}}$ (c) $\Re(u^{\text{true}})$: $\tilde{\mu} = 10$, $\tilde{g}_{\text{II}}$

(d) $\tilde{\mu}$ sweep, $\tilde{g}_{\text{I}}$

Figure 1. The truth solutions associated with the 2D Helmholtz problem. (a) $\Re(u^{\text{true}})$: $\tilde{\mu} = 2, \tilde{g}_{\text{I}}$. (b) $\Re(u^{\text{true}})$: $\tilde{\mu} = 10, \tilde{g}_{\text{I}}$. (c) $\Re(u^{\text{true}})$: $\tilde{\mu} = 10, \tilde{g}_{\text{II}}$. (d) $\tilde{\mu}$ sweep, $\tilde{g}_{\text{I}}$.

3.3. Best-knowledge model and PBDW spaces

We consider the parameterized best-knowledge model $G^\mu(w, v) \equiv f^\mu_{g\equiv 0}(v) - a^\mu(w, v)$ for $\mu \in \mathcal{D} \equiv [2, 10]$. The associated best-knowledge solution is $u^{\text{bk},\mu} = \Upsilon^\mu_{g\equiv 0}$, $\mu \in \mathcal{D}$. We then construct the background spaces $\mathcal{Z}_N$, $N = 1, \ldots, N_{\max}$, using the $\textsc{WeakGreedy}_N$ procedure described in Algorithm 1. For simplicity, we use the dual norm of the residual as the error estimate: $\Delta^{\text{bk},\mu}_N \equiv \inf_{w\in\mathcal{Z}_N} \sup_{v\in\mathcal{U}^{\mathcal{N}}} |G^\mu(w, v)|/\|v\|$ (see [29] for details). The $N_{\max} = 7$ parameter points chosen by the $\textsc{WeakGreedy}_N$ algorithm are, in order, $(10.00, 2.00, 4.50, 3.15, 6.35, 9.40, 8.65)$.

As previously discussed, the important property of $\mathcal{Z}_N$ is that it approximates the best-knowledge parametric manifold in the sense that the discretization error $\epsilon^{\text{bk}}_{\text{disc},N} \equiv \sup_{w\in\mathcal{M}^{\text{bk}}} \|w - \Pi_{\mathcal{Z}_N} w\|$ is small. We show in Figure 2 the convergence of the discretization error as a function of the dimension of N. The error decreases exponentially with N. We also note that the residual-based error estimate, $\Delta^{\text{bk},\mu}_N$, while not a rigorous bound, serves as an indicator of the true discretization error.

We now discuss the construction of the experimentally observable space $\mathcal{U}_M$. We model the (synthetic) observations by a Gaussian convolution with a standard deviation of $r_m = 0.02$: $\ell^{\text{o}}_m(\cdot) = \text{Gauss}(\cdot, x^{\text{c}}_m, r_m = 0.02)$. We then consider experimentally observable spaces $\mathcal{U}_M$, $M = 1, \ldots, M_{\max}$, based on two different sets of observation centers $\{x^{\text{c}}_m\}^M_{m=1}$: randomly selected $\textsc{RandomUniform}_M$ centers and (approximately) stability-maximizing $\textsc{SGreedy}^{\text{local}}_M$ centers. The first 20 centers for each set are shown in Figure 3(a, b). We also show in Figure 3(c) an example of an experimentally observable function. The function, while concentrated about $x^{\text{c}}_{m=3}$, has a non-compact support; in particular, $(R_{\mathcal{U}}\ell^{\text{o}}_{m=3})(x) \in [0.86, 1.45]$, $\forall x \in \Omega$, and the function does not vanish anywhere in the domain.

As previously discussed, the space $\mathcal{U}_M$ must satisfy two criteria: maximization of the stability constant $\beta_{N,M}$ and approximation of the unanticipated uncertainty space $\mathcal{Z}^\perp_N$. Here, we focus on the assessment of the former. We show in Figures 4(a, b) the stability constant $\beta_{N,M}$ associated with

DOI: 10.1002/nme

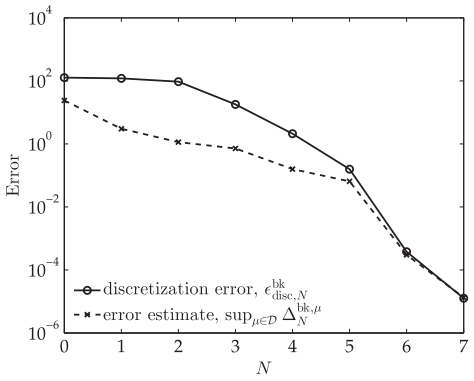

Figure 2. Convergence of the $\textsc{WeakGreedy}_N$ algorithm.

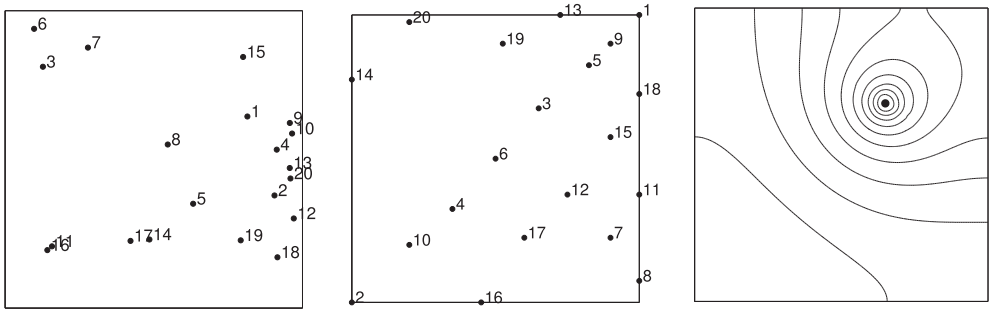

(a) $\textsc{RandomUniform}_M$ (b) $\textsc{SGreedy}^{\text{local}}_M$ (c) $R_{\mathcal{U}}\ell^{\text{o}}_{m=3}$ ($\textsc{SGreedy}^{\text{local}}_M$)

Figure 3. Observation centers selected by (a) $\textsc{RandomUniform}_{M=20}$ and (b) $\textsc{SGreedy}^{\text{local}}_{M=20}$; (c) an experimentally observable function $R_{\mathcal{U}}\ell^{\text{o}}_{m=3}$ in $\mathcal{U}_M$.

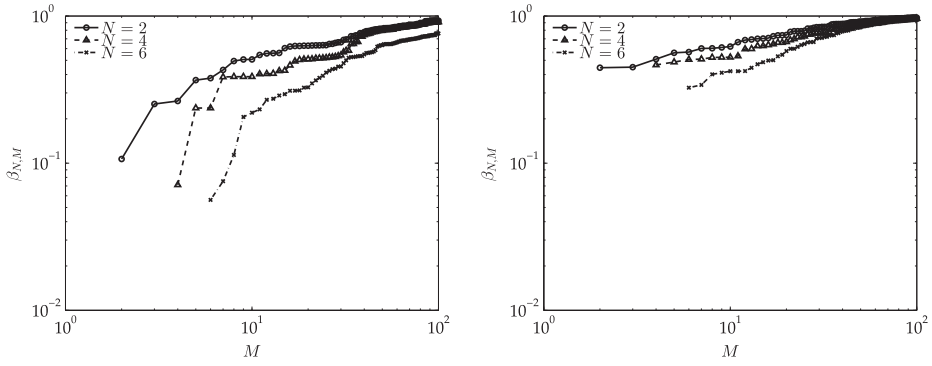

(a) $\textsc{RandomUniform}_M$ (b) $\textsc{SGreedy}^{\text{local}}_M$

Figure 4. Behavior of the stability constant for (a) $\textsc{RandomUniform}_M$ and (b) $\textsc{SGreedy}^{\text{local}}_M$ observation centers.

$\textsc{RandomUniform}_M$ and $\textsc{SGreedy}^{\text{local}}_M$ centers, respectively, for a few different N as a function of M. We observe that the $\textsc{SGreedy}^{\text{local}}_M$ algorithm provides a much better stability constant, in particular for a small M.

3.4. Error analysis

3.4.1. Case I: perfect model. We first consider case I: the case with a perfect best-knowledge model. As mentioned, for this case, $u^{\text{true}} \in \mathcal{M}^{\text{bk}}$ and $u^{\text{true}} = u^{\text{bk},\tilde{\mu}} = \Upsilon^{\tilde{\mu}}_{g\equiv 0}$ for some $\tilde{\mu} \in \mathcal{D}$. Hence,

DOI: 10.1002/nme

we have no model error, $\epsilon^{\mathrm{bk}}_{\mathrm{mod}}(u^{\mathrm{true}}) = 0$; however, we still have a finite discretization error $\epsilon^{\mathrm{bk}}_{\mathrm{disc},N}$ because $\mathcal{M}^{\mathrm{bk}} \not\subset \mathcal{Z}_N$ for a finite N.

We show in Figure 5(a) the variation in the maximum relative error over the parameter domain as a function of the number of observations M for a few different values of N. For this case with a perfect model—as predicted from the *a priori* bound in Proposition 2 and the rapid convergence of the discretization error $\epsilon^{\mathrm{bk}}_{\mathrm{disc},N}$ in Figure 2—the error decreases rapidly with N as

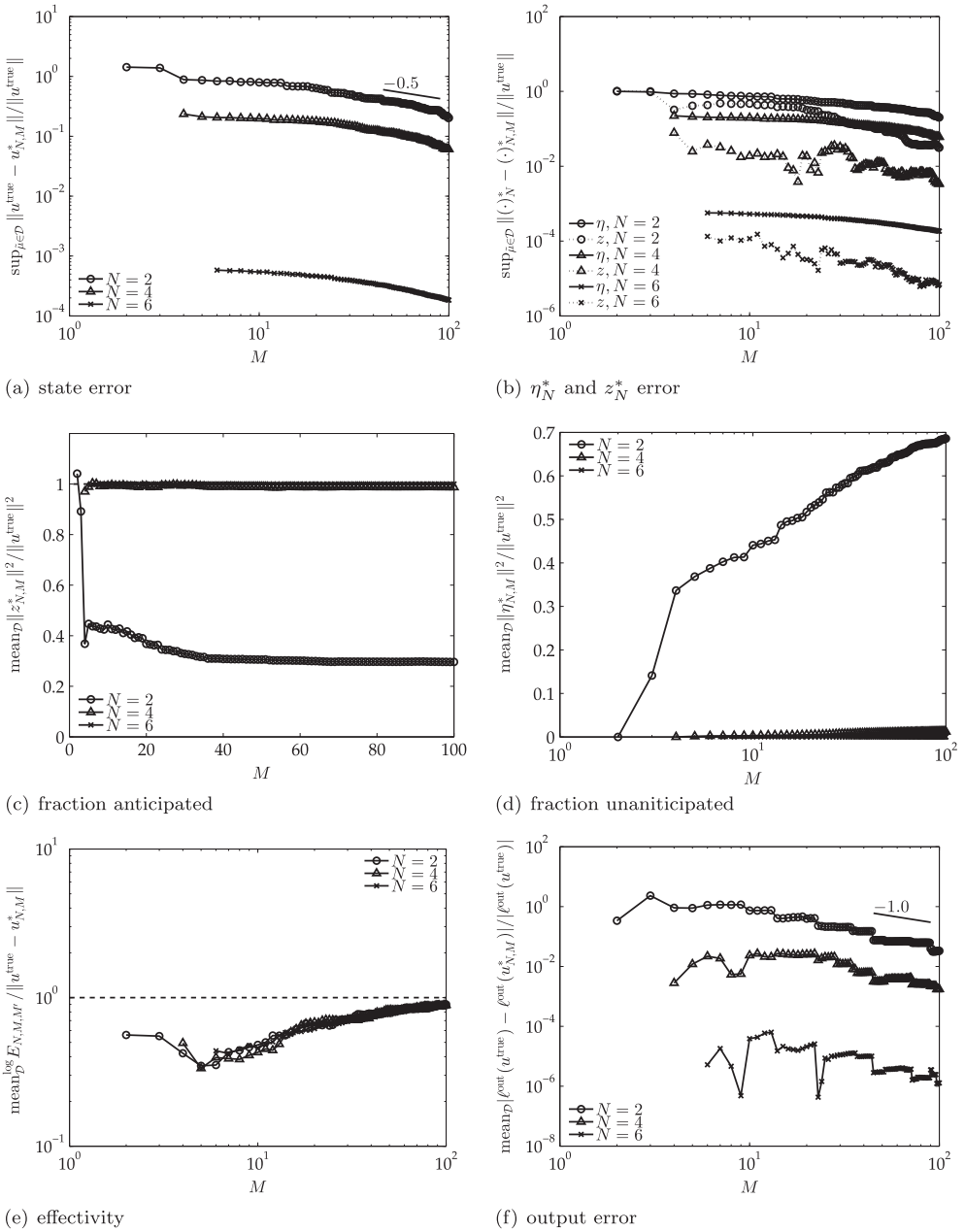

Figure 5. Case I. Behavior of (a) the maximum relative error over the parameter domain, (b) the maximum error for the update and background components, (c) the anticipated fraction of the state, (d) the unanticipated fraction of the state, (e) the log-mean *a posteriori* error estimate effectivity (for $M' = 2M$), and (f) the mean relative output error, as a function of the number of observations M for a few different values of N using $\texttt{SGREEDY}^{\mathrm{local}}_{M}$ observation centers.

DOI: 10.1002/nme

$\epsilon_N^{\text{bk}}(u^{\text{true}}) \equiv \inf_{z\in\mathcal{Z}_N} \|u^{\text{true}} - z\|$ decreases rapidly. Hence, the experimentally observable space $\mathcal{U}_M$, $M \geq N$, is required only to provide stability and not to complete the deficiency in the background space $\mathcal{Z}_N$ for a sufficiently large (and in practice moderate) N.

In order to understand in more detail the error behavior, we show in Figure 5(b) the convergence of the two components of the PBDW estimate: $z^*_{N,M} \in \mathcal{Z}_N$—the background component of the estimate—and $\eta^*_{N,M} \in \mathcal{U}_M \cap \mathcal{Z}_N^\perp$—the update component of the estimate. We observe that the error in $z^*_{N,M}$ is typically smaller than the error in $\eta^*_{N,M}$. Note that this is not a contradiction with Proposition 2, which provides *bounds* for the errors in $z^*_{N,M}$ and $\eta^*_{N,M}$.

We in addition show in Figure 5(c, d) the fraction of the state anticipated and unanticipated, respectively, by the parameterized best-knowledge model. As there is no model error ($\epsilon_{\text{mod}}^{\text{bk}}(u^{\text{true}}) = 0$), the unanticipated fraction vanishes as $N \to \infty$.

We show in Figure 5(e) the variation in the *a posteriori* error estimate effectivity, $E_{N,M,M'}/\|u^{\text{true}} - u^*_{N,M}\|$, as a function of M and N for $M' = 2M$. The error estimate unfortunately underestimates the true error. However, the effectivity approaches unity as M (and hence M') increases.

We finally show in Figure 5(f) the convergence of the PBDW output estimates. As we have observed for the $\|\cdot\|$-norm of the error, we observe a rapid convergence of the output error with N for this case with a perfect model. In addition, as predicted by Proposition 3, we observe superconvergence with M: the output error decreases as M^{-1} as opposed to $M^{-1/2}$ for the state error.

3.4.2. Case II: imperfect model. We now consider the truths u^{true} with $\tilde{g} = \tilde{g}_{\text{II}} \neq 0$ such that the parameterized best-knowledge model based on $\tilde{g} \equiv 0$ is inconsistent with the truths. In other words, the model error $\epsilon_{\text{mod}}^{\text{bk}}(u^{\text{true}}) \neq 0$ and $u^{\text{true}} \notin \mathcal{M}^{\text{bk}}$. Proposition 2 predicts that, as $\epsilon_N^{\text{bk}}(u^{\text{true}}) \equiv \inf_{z\in\mathcal{Z}_N} \|u^{\text{true}} - z\|$ does not converge to 0, we must rely on the relatively slow convergence with M provided by $\inf_{q\in\mathcal{U}_M\cap\mathcal{Z}_N^\perp} \|\Pi_{\mathcal{Z}_N^\perp} u^{\text{true}} - q\|$. Figure 6(a) confirms that this indeed is the case; while the error decreases with N, the decrease is not as rapid as that observed for the perfect model in case I. We observe that the error converges at the rate of $M^{-1/2}$, and in fact, we must rely on this rather slow convergence, and not the rapid convergence with N, to obtain a good estimate.

We observe in Figure 6(b) that, in the case of imperfect models, the error in $\eta^*_{N,M}$ dominates over the error in $z^*_{N,M}$. This is consistent with the fact that $\|\eta^*_N\|$ does not decrease rapidly with N for an imperfect model. We confirm in Figure 6(c, d) that this indeed is the case: because model error $\epsilon_{\text{mod}}^{\text{bk}}(u^{\text{true}}) \neq 0$, the fraction of the state unanticipated by the parameterized best-knowledge model does not vanish even if $N \to \infty$. We show in Figure 6(e) that the *a posteriori* error estimate in case II works as well as it does in case I. We finally observe in Figure 6(f) that the output error, like the state error, does not decrease rapidly with N but, unlike the state error, superconverges with M at the rate of M^{-1}.

We finally assess the effect of observation centers on the state estimates. We show in Figure 7(a) the convergence of the state estimation error using the $\textsc{RandomUniform}_M$ observation centers. Compared with the results shown in Figure 6(a) obtained using the $\textsc{SGreedy}_M^{\text{local}}$ observation centers, we observe an increase in the error in particular for a small M. To understand the cause of the increased error, we show in Figure 7(b) the decomposition of the error into the background and update components; we then compare the results with that shown in Figure 6(b) obtained using the $\textsc{SGreedy}_M^{\text{local}}$ observation centers. We note that in general the error in the update component $\eta^*_{N,M}$ is not strongly affected by the choice of the observation centers; this is consistent with Proposition 2, which states that the estimation of η^*_N is independent of the stability constant $\beta_{N,M}$, which strongly depends on the observation centers as shown in Figure 4(a, b). On the other hand, we note that the error in the background component $z^*_{N,M}$ is much larger for the $\textsc{RandomUniform}_M$ observation centers than for the $\textsc{SGreedy}_M^{\text{local}}$ observation centers, especially for a small M. This again is consistent with Proposition 2, which shows that the stability constant $\beta_{N,M}$ plays a crucial role in the estimation of z^*_N.

DOI: 10.1002/nme

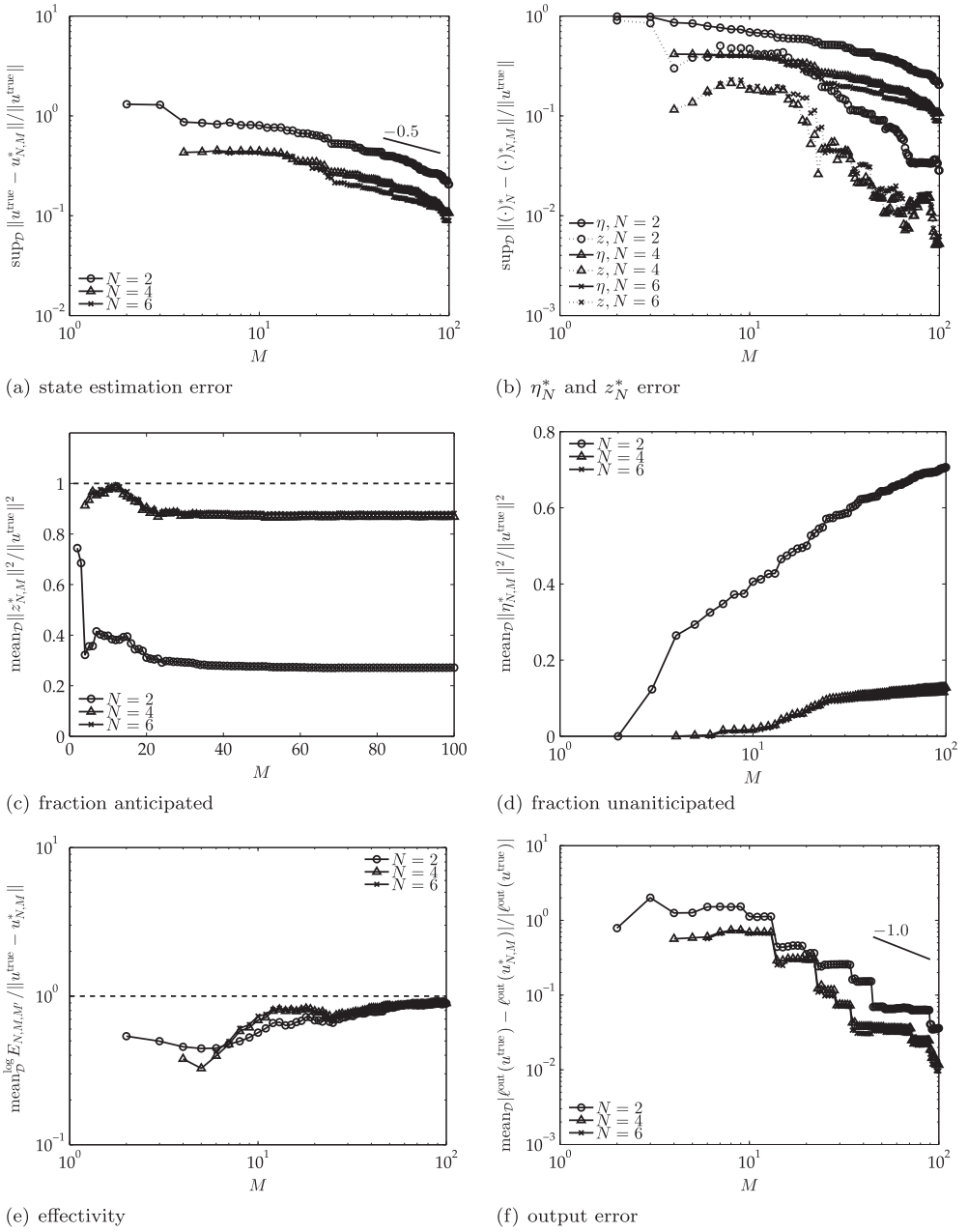

Figure 6. Case II. Behavior of (a) the maximum relative error over the parameter domain, (b) the maximum error for the update and background components, (c) the anticipated fraction of the state, (d) the unanticipated fraction of the state, (e) the log-mean *a posteriori* error estimate effectivity (for $M' = 2M$), and (f) the mean relative output error, as a function of the number of observations M for a few different values of N using $\texttt{SGREEDY}^{\text{local}}_{\boldsymbol{M}}$ observation centers.

4. PHYSICAL PROBLEM: RAISED-BOX ACOUSTIC RESONATOR

4.1. Physical system

We now consider the application of the PBDW framework to a physical system: a raised-box acoustic resonator. In particular, we wish to estimate the (time-harmonic) pressure field inside the raised-box acoustic resonator described as a complex field in the frequency domain.

DOI: 10.1002/nme

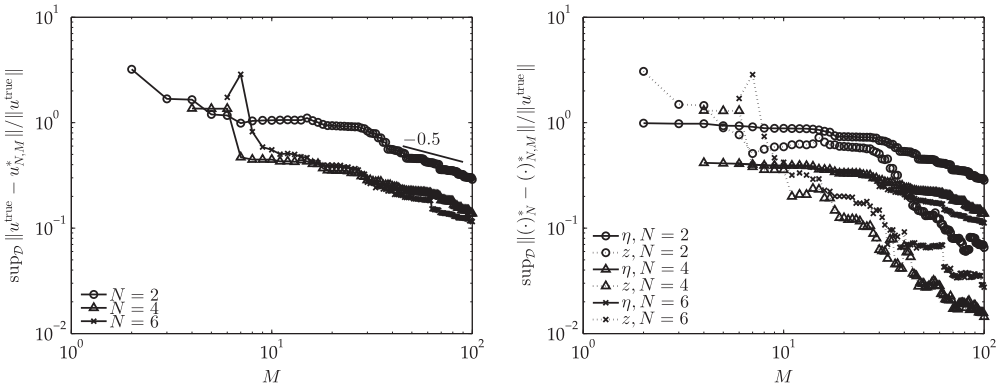

(a) state error (b) η_N^* and z_N^* error

Figure 7. Case II. Behavior of (a) the maximum relative error over the parameter domain and (b) the maximum error for the update and background components, as a function of the number of observations M for a few different values of N using $\textsc{RandomUniform}_M$ observation centers.

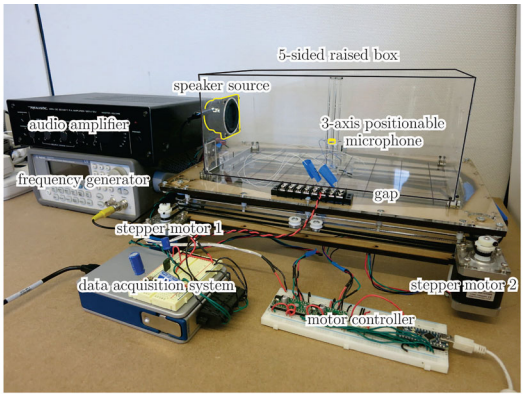

(a) robotic observation platform

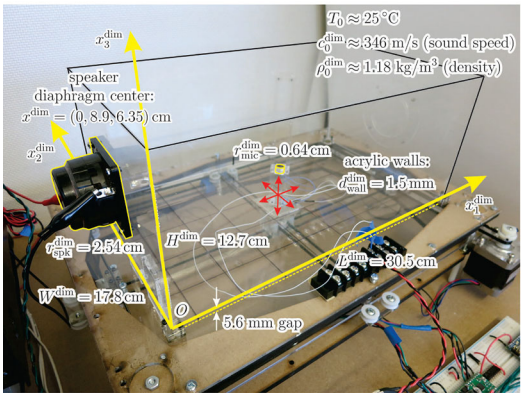

(b) raised-box acoustic resonator

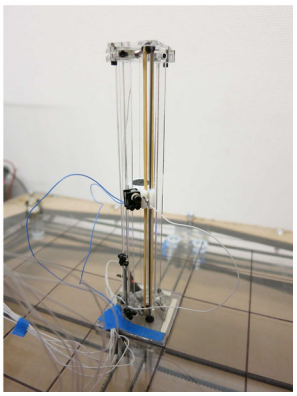

(c) microphone holder

Figure 8. Configuration of (a) the Robotic Observation Platform, (b) the raised-box acoustic resonator, and (c) the microphone holder.

We show in Figure 8(a) the physical system: a five-sided, raised, acrylic box is separated from a bottom panel by a small gap that permits acoustic radiation from the raised-box interior to the exterior; a speaker (Tang Band W2-1625SA, Tang Band Ltd., Taipei, Taiwan) mounted in the center of one side of the box provides a sound source at a single prescribed frequency $\tilde{f}^{\text{dim}}$. Here $\tilde{\cdot}$ indicates

DOI: 10.1002/nme

that the frequency is specified and measured by the frequency generator; also, superscript 'dim' refers to a dimensional variable. We show in Figure 8(b) the dimensional values of the geometric and thermodynamic variables that define the physical system.

4.2. Robotic Observation Platform

4.2.1. Data acquisition. To permit autonomous, rapid, and accurate data acquisition, we design and build a Robotic Observation Platform for the raised-box acoustic resonator.

As shown in Figure 8(a), a microphone (RadioShack model 270-092, RadioShack Corporation, Fort Worth, TX) attached to a three-axis positionable holder measures the pressure at a specified position inside the raised box. Actuation of the microphone in the x_1 and x_2 directions (as defined in Figure 8(b)) is provided by two stepper motors controlling a belt-driven output (not shown) that is magnetically coupled to the microphone holder shown in Figure 8(c) through the bottom panel. Actuation of the microphone in the x_3 direction is provided by a small DC motor mounted to the microphone holder that positions the microphone via potentiometer position feedback.

Figure 8(a) also shows the frequency generator and audio amplifier used to control the output of the speaker, the motor controller used to control the stepper and DC motors, and the data acquisition system used to capture the measured speaker input and microphone output.

A typical experiment consists of positioning the microphone in three dimensions, generating a sequence of tones at prescribed frequencies using the frequency generator, amplifier, and speaker, and recording the speaker input and microphone output using the data acquisition system. The microphone is then repositioned, and the process is repeated.

Prior to use, the microphone was calibrated over the frequency range of interest using a sound level calibrator (Reed SC-05, REED Instruments, Sainte-Anne-de-Bellevue, Canada) accurate to within 6%, a sound level meter (Extech 407730, Extech Instruments, Nashua, NH), and a reference microphone (Dayton Audio EMM-6, Springboro, OH) with a known frequency response accurate to within 1%. The measured calibration curve of the microphone and its custom microphone preamplifier circuit is shown in Figure 9.

4.2.2. Data reduction. We briefly discuss our data reduction procedure. We focus here on the data reduction of a single speaker–microphone observation pair; to obtain M observations, we repeat the procedure M times.

The microphone generates a voltage signal $\varphi^{\mathrm{dim}}_{\mathrm{mic}}(x^{\mathrm{dim}}, t^{\mathrm{dim}})$ as a function of time t^{dim} at a given location x^{dim} within the box. We then assume that the measured voltage is of the form $\varphi^{\mathrm{dim}}_{\mathrm{mic}}(x^{\mathrm{dim}}, t^{\mathrm{dim}}_j) = \Re\{\Phi^{\mathrm{dim}}_{\mathrm{mic}}(x^{\mathrm{dim}}; \tilde{f}^{\mathrm{dim}}) e^{i2\pi \tilde{f}^{\mathrm{dim}} t^{\mathrm{dim}}_j}\} + \epsilon^{\mathrm{dim}}_{\mathrm{mic}}(x^{\mathrm{dim}}, t^{\mathrm{dim}}_j)$, $j = 1, \ldots, M'$, where $\Phi^{\mathrm{dim}}_{\mathrm{mic}}(x^{\mathrm{dim}}; \tilde{f}^{\mathrm{dim}}) \in \mathbb{C}$ is the complex microphone voltage, $\epsilon^{\mathrm{dim}}_{\mathrm{mic}}(x^{\mathrm{dim}}, t^{\mathrm{dim}}_j) \in \mathbb{R}$ is the noise, and M' is the number of measurements in the time series. We take $M' = 4000$ measurements in our experiment. We then assume that $\epsilon^{\mathrm{dim}}_{\mathrm{mic}}(x^{\mathrm{dim}}, t^{\mathrm{dim}}) \sim \mathcal{N}(0, (\sigma^{\mathrm{dim}}_{\mathrm{mic}}(x^{\mathrm{dim}}; \tilde{f}^{\mathrm{dim}}))^2)$ and perform linear

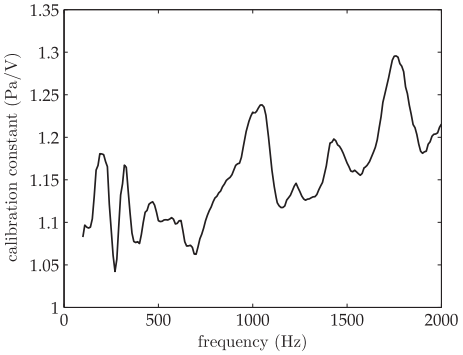

Figure 9. Measured calibration curve of the microphone (RadioShack model 270-092) and preamplifier.

DOI: 10.1002/nme

regression to identify the complex microphone voltage $\Phi^{\text{dim}}_{\text{mic}}(x^{\text{dim}}; \tilde{f}^{\text{dim}}) \in \mathbb{C}$ and the noise standard deviation $\sigma^{\text{dim}}_{\text{mic}}(x^{\text{dim}}; \tilde{f}^{\text{dim}}) \in \mathbb{R}_{>0}$.

We apply a similar data reduction procedure to the speaker voltage signal $\varphi^{\text{dim}}_{\text{spk}}(\tilde{f}^{\text{dim}})$ to deduce the complex speaker velocity $\Phi^{\text{dim}}_{\text{spk}}(\tilde{f}^{\text{dim}}) \in \mathbb{C}$ and the associated standard deviation $\sigma^{\text{dim}}_{\text{spk}}(\tilde{f}^{\text{dim}}) \in \mathbb{R}_{>0}$. We emphasize that we measure the microphone voltage $\varphi^{\text{dim}}_{\text{mic}}(x^{\text{dim}}, t^{\text{dim}})$ and the speaker voltage $\varphi^{\text{dim}}_{\text{spk}}(t^{\text{dim}})$ simultaneously over the same period; we appeal to this simultaneous data acquisition to deduce the phase information of the pressure signal from a single microphone observation, as described shortly.

Once we obtain the speaker–microphone voltage pair $(\Phi^{\text{dim}}_{\text{spk}}, \Phi^{\text{dim}}_{\text{mic}})$, we calculate the associated speaker velocity and microphone pressure. We model the speaker as a harmonic oscillator to identify the (frequency-dependent) transfer function from the applied speaker voltage $\Phi^{\text{dim}}_{\text{spk}}$ to the resultant speaker velocity $V^{\text{dim}}_{\text{spk}}$; the construction of the transfer function is discussed in Section 4.3. We convert the microphone voltage $\Phi^{\text{dim}}_{\text{mic}}$ to the associated pressure $P^{\text{dim}}_{\text{mic}}$ using the calibration curve shown in Figure 9.

We finally introduce the following normalized quantities: the coordinate, $x \equiv x^{\text{dim}}/r^{\text{dim}}_{\text{spk}}$; the frequency, $\tilde{k} \equiv 2\pi \tilde{f}^{\text{dim}} r^{\text{dim}}_{\text{spk}}/c^{\text{dim}}_0$; and the complex pressure observed by a microphone centered at x^{c}_m, $P^{\text{obs}}(x^{\text{c}}_m; \tilde{k}) \equiv (P^{\text{dim}}_{\text{mic}}(x^{\text{c}}_m; \tilde{f}^{\text{dim}})/V^{\text{dim}}_{\text{spk}}(\tilde{f}^{\text{dim}}))/(\rho^{\text{dim}}_0 c^{\text{dim}}_0)$. Here, ρ^{dim}_0 is the density of the air, and c^{dim}_0 is the speed of sound.

Note that, in our normalization of the pressure, the initial (arbitrary) phase angle of the (complex) speaker velocity cancels out (and subsequently becomes irrelevant) as it appears in $P^{\text{dim}}_{\text{mic}}$ in the numerator and $V^{\text{dim}}_{\text{spk}}$ in the denominator. It is important to note that we may thus obtain phase information throughout the pressure field with just a single movable microphone, a substantial advantage in the real-time context as implemented in our Robotic Observation Platform. We shall exploit phase as a sensitive error metric for our data assimilation procedure.

We comment on the precision of typical experimental data. We show in Figure 10 a time trace of typical regression for the speaker and microphone. The estimate of the complex amplitude for the speaker voltage is $0.266 + 0.324i$ V, and the associated standard deviation is 0.00095 V; the signal-to-noise ratio is 443. The estimate of the complex amplitude for the microphone voltage is $-0.319 - 0.140i$ V, and the associated standard deviation is 0.00185 V; the signal-to-noise ratio is 189. Note that because for a given frequency the voltage-to-pressure calibration is linear, the signal-to-noise ratio of the voltage directly applies to the pressure. We conclude that the noise associated with any given observation is small. In addition, because the signal-to-noise ratio of the speaker voltage, which is used in normalization, is high, we expect the normalized pressure P^{obs} to inherit this signal-to-noise ratio.

We continue the assessment of the precision of the data, in particular reproducibility and environmental control, through a repetition test. We show in Figure 11 the typical normalized pressure

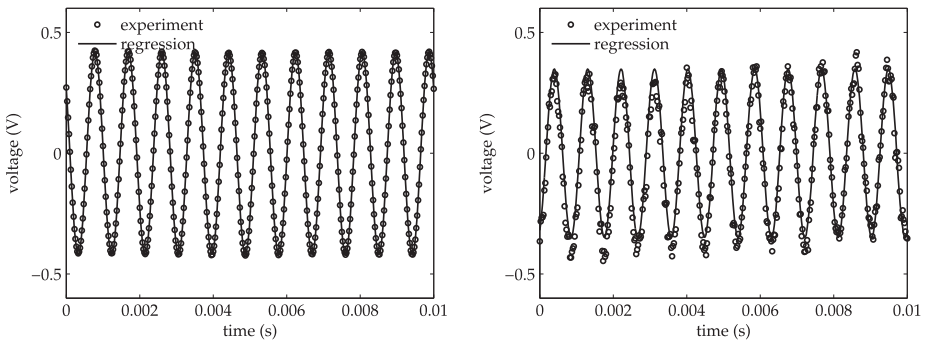

(a) speaker (b) microphone

Figure 10. A time trace of typical raw data and regression estimate over the first 0.01 s; the data acquisition period is 10 times longer ($x^{\text{dim}} = (27.9, 15.2, 1.3)$ cm, $\tilde{f}^{\text{dim}} = 1100$ Hz). (a) Speaker. (b) Microphone.

DOI: 10.1002/nme

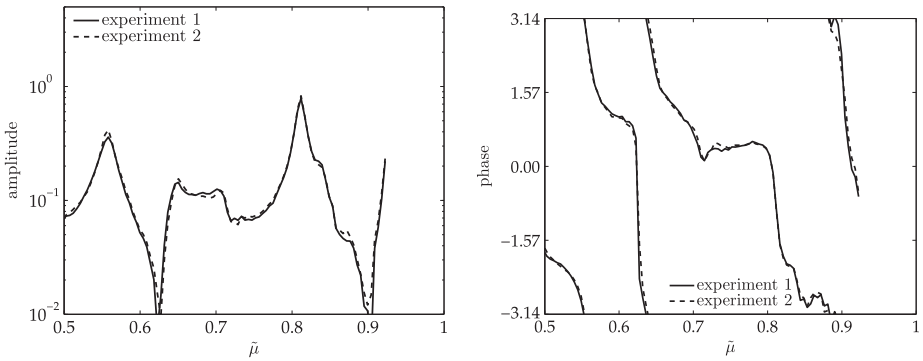

(a) amplitude (b) phase

Figure 11. Comparison of the normalized pressures obtained in two different experiments ($x^{\text{dim}} = (27.9, 15.2, 1.3)$ cm). (a) Amplitude. (b) Phase.

observed in two different experiments. The microphone was moved to the location following two different paths; hence, the comparison captures any hysteresis that might be present in the microphone positioning system. We observe that the two results closely match each other. The comparison suggests that the physical pressure field is invariant in the sense that within a given set of observations, we maintain environmental conditions such as the temperature.

The calibration of Section 4.2.1 ensures accurate microphone pressure measurement; the regression results and associated signal-to-noise ratio suggest very little noise associated with the (effectively) Fourier transform of the temporal signal; and finally, the repetition test indicates good control of position and environmental conditions and hence very little systematic error. As regards the latter, we also note that the microphone dimension is small compared with the wavelength of the acoustic waves, and hence, any sufficiently small choice for r_m suffices; we further note that the instrument holder of Figure 8(c) is largely acoustically invisible, in particular because of the thin profile and light vertical-drive mechanism.

We conclude the following: (i) for our purposes here, we may indeed apply the 'noise-free' observation framework developed in the previous sections, and (ii) for purposes of assessment, we may equate our experiments to the true field.

4.2.3. Dataset. We consider 92 configurations associated with the frequency of $\tilde{f}^{\text{dim}} = 1090, \ldots, 2000$ Hz; the associated normalized frequency based on the ambient temperature, $\tilde{k}$, takes on a value in $[0.502, 0.921]$. We acquire data at 84 spatial points distributed on a Cartesian grid:

$$x_m^{\text{c}} \in \Xi \equiv \{1.00, 2.67, 4.33, 6.00, 7.67, 9.33, 11.00\} \times \{1.00, 2.67, 4.33, 6.00\} \times \{0.50, 2.50, 4.50\}.$$

We then apply the data reduction procedure described earlier to compute $P^{\text{obs}}(x_m^{\text{c}}; \tilde{k})$.

We recall that the regression analysis and repeatability test suggest that the noise in the pressure observations is in fact small. We hence employ the dataset for two purposes. First, we use the dataset as experimental observations from which to construct the PBDW estimate; in fact, because the noise is small, we may apply the noise-free formulation and theory developed in Section 2. Second, we use the dataset as a surrogate for the truth with which to assess the accuracy of the PBDW estimate $P^{\text{true}}(x_m^{\text{c}}; \tilde{k}) \equiv P^{\text{obs}}(x_m^{\text{c}}; \tilde{k})$; we recall that our goal is prediction of the true state, and not just the experimental observations—the two coincide only in the noise-free case.

4.3. Best-knowledge model

The geometry of the mathematical model is shown in Figure 12. We recall that our goal is to approximate the pressure field everywhere inside the raised box, $\Omega =]0, 12[\times]0, 7[\times]0, 5[$, where we recall the nondimensionalization $x \equiv x^{\text{dim}}/r_{\text{spk}}^{\text{dim}}$. We in addition introduce a superdomain for the best-knowledge model, $\Omega^{\text{bk}} \supset \Omega$, that includes the regions both inside and outside of the box such that we may model the radiation from the bottom gap of the box.

DOI: 10.1002/nme

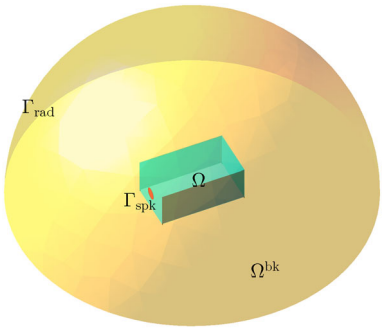

Figure 12. Geometry of the computational model. Here, Ω is the domain inside of the raised box, Ω^{bk} is the (extended) computational domain that includes the regions inside and outside of the raised box, Γ_{spk} is the speaker boundary, and Γ_{rad} is the radiation boundary.

We now define our parameterized best-knowledge model over the extended domain Ω^{bk}. The sole parameter of our best-knowledge model is the nondimensional wavenumber, $\mu \equiv k \equiv 2\pi f^{\text{dim}} r_{\text{spk}}^{\text{dim}}/c_0^{\text{dim}}$; the associated parameter domain is $\mathcal{D} = [0.5, 1.0]$. We then seek the nondimensionalized complex pressure field $u^{\text{bk},\mu} \equiv P^{\text{dim}}/(\rho_0^{\text{dim}} c_0^{\text{dim}} V_{\text{spk}}^{\text{dim,bk}}(k))$. The field is governed by a weak statement: find $u^{\text{bk},\mu} \in \mathcal{U}^{\text{bk}} \equiv H^1(\Omega^{\text{bk}})$ such that

$$G^\mu(u^{\text{bk},\mu}, v) \equiv f^\mu(v) - a^\mu(u^{\text{bk}}, v) = 0 \quad \forall v \in \mathcal{U}^{\text{bk}}$$

where

$$a^\mu(w, v) \equiv \int_\Omega \nabla w \cdot \nabla \bar{v} dx - \mu^2 \int_\Omega w \bar{v} dx + \left(i\mu + \frac{1}{R}\right) \int_{\Gamma_{\text{rad}}} w \bar{v} ds \quad \forall w, v \in \mathcal{U},$$
$$f^\mu(v) \equiv i\mu \int_{\Gamma_{\text{spk}}} 1 \, \bar{v} ds \quad \forall v \in \mathcal{U}.$$

We model the harmonic excitation generated by the speaker by a uniform Neumann condition over Γ_{spk}; note that, under our normalization, the speaker velocity is unity. We model the radiation into free space by a first-order accurate radiation boundary condition on Γ_{rad}. Thanks to the radiation term, the problem is well posed for any $\mu \in \mathcal{D}$. We approximate the solution in a 35,325-element $\mathbb{P}^3$ finite element space.

We briefly discuss our speaker model. We model the speaker as a harmonic oscillator driven by an electromagnetic voice coil. The frequency-dependent transfer function of the speaker diaphragm velocity $V_{\text{spk}}^{\text{dim}}$ with respect to the speaker input voltage $\Phi_{\text{spk}}^{\text{dim}}$ in terms of the voice coil BL product $(BL)_{\text{spk}}^{\text{dim}}$, the voice coil electrical resistance $R_{\text{e, spk}}^{\text{dim}}$, the voice coil electrical inductance $L_{\text{e, spk}}^{\text{dim}}$, the speaker suspension stiffness $k_{\text{spk}}^{\text{dim}}$, the speaker moving mass $m_{\text{spk}}^{\text{dim}}$, and the speaker mechanical damping $b_{\text{spk}}^{\text{dim}}$ is then given by

$$\frac{V_{\text{spk}}^{\text{dim}}}{\Phi_{\text{spk}}^{\text{dim}}} = \frac{(BL)_{\text{spk}}^{\text{dim}} i 2\pi f^{\text{dim}}}{\left(R_{\text{e, spk}}^{\text{dim}} + i 2\pi f^{\text{dim}} L_{\text{e, spk}}^{\text{dim}}\right)\left(k_{\text{spk}}^{\text{dim}} - m_{\text{spk}}^{\text{dim}} (2\pi f^{\text{dim}})^2 + i 2\pi f^{\text{dim}} b_{\text{eff, spk}}^{\text{dim}}\right)}$$

where we define the effective damping of the speaker as

$$b_{\text{eff, spk}}^{\text{dim}} = b_{\text{spk}}^{\text{dim}} + \frac{\left((BL)_{\text{spk}}^{\text{dim}}\right)^2}{R_{\text{e, spk}}^{\text{dim}} + i 2\pi f^{\text{dim}} L_{\text{e, spk}}^{\text{dim}}}.$$

Experiments were conducted to measure the various speaker parameters, yielding values that differ from the manufacturer-specified values. Both sets of values are listed in Table I. The transfer function of the speaker for the measured parameter values is shown in Figure 13.

DOI: 10.1002/nme

Table I. Manufacturer-specified and measured speaker parameters.

Parameter	Specified value	Measured value	Units
$R^{\text{dim}}_{\text{e, spk}}$	6.6	7.2	Ω
$L^{\text{dim}}_{\text{e, spk}}$	2.15×10^{-4}	2.64×10^{-4}	H
$(BL)^{\text{dim}}_{\text{spk}}$	5.16	5.4	T · m
$k^{\text{dim}}_{\text{spk}}$	772.2	1410.8	N/m
$m^{\text{dim}}_{\text{spk}}$	2.3×10^{-3}	3.4×10^{-3}	kg
$b^{\text{dim}}_{\text{spk}}$	0.05	0.24	N · s/m

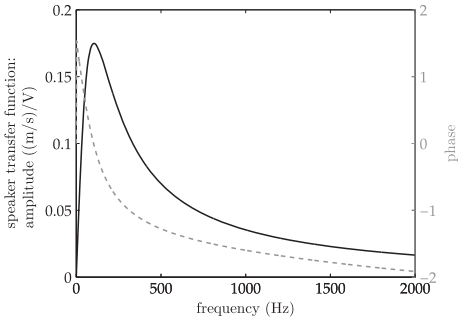

Figure 13. Speaker (Tang Band W2-1625SA) transfer function (magnitude and phase) for the measured parameter values.

4.4. PBDW spaces

4.4.1. Function space $\mathcal{U}$. We introduce a Hilbert space $\mathcal{U} \equiv H^1(\Omega)$ endowed with a weighted H^1 inner product and norm,

$$(w, v) \equiv \int_\Omega \nabla w \cdot \nabla \bar{v} dx + \kappa^2 \int_\Omega w \bar{v} dx \quad \text{and} \quad \|w\| \equiv \sqrt{(w, w)},$$

for a reference wavenumber $\kappa = 0.5$. The reference wavenumber is chosen to induce an update function $q_m \equiv R_{\mathcal{U}_M} \ell^{\text{o}}_m$ with a spatial decay on the order of the wavelength.

4.4.2. Background spaces $\mathcal{Z}_N$. We employ the superdomain formulation described in Section 2.7.3. We first apply the weak greedy algorithm described in Algorithm 1 to form $\texttt{WeakGreedy}_N(\mathcal{M}^{\text{bk}}) \rightarrow \mathcal{Z}^{\text{bk}}_N$, $N = 1, \ldots, 15 \equiv N_{\max}$. We then restrict the functions in $\mathcal{Z}^{\text{bk}}_N$ to the domain of interest to form $\mathcal{Z}_N = \{z \in \mathcal{U} | \; z = z^{\text{bk}}|_\Omega, \; z^{\text{bk}} \in \mathcal{Z}^{\text{bk}}_N\}$. We emphasize that $\mathcal{Z}_N \subset \mathcal{U}$ is defined over Ω, not the (extended) best-knowledge domain Ω^{bk}.

4.4.3. Experimentally observable update spaces $\mathcal{U}_M$. We model the experimental observations provided by the microphone with Gaussians. Specifically, we consider $\ell^{\text{o}}_m(\cdot) = \text{Gauss}(\cdot; x^{\text{c}}_m, r_m = 0.2)$. We choose a standard deviation r_m that is consistent with an approximate filter width of the microphone; however, because the spatial extent of the microphone is small compared with the pressure wavelength, the precise choice of r_m is not too important. The associated library is of the form $\mathcal{L} = \{\ell \in \mathcal{U}' \mid \ell(\cdot) = \text{Gauss}(\cdot; x^{\text{c}}_m, r_m), \; x^{\text{c}}_m \in \Xi\}$; note that we guarantee by construction that the observation points are in Ξ, and hence, the associated data are in the dataset. We then obtain $\mathcal{U}_M = \texttt{SGreedy}_M(\mathcal{Z}_{N_{\max}})$, $M = 1, \ldots, 48 \equiv M_{\max}$.

DOI: 10.1002/nme

4.5. Real-time in situ data assimilation

We briefly summarize the timing associated with the online data acquisition and data assimilation. The Robotic Observation Platform requires approximately 3 s per observation to reposition the microphone and to take the pressure measurement. The solution of the PBDW saddle system

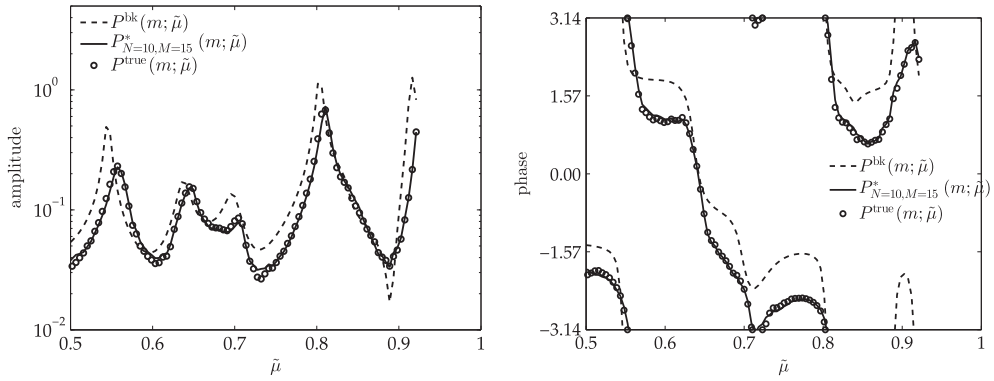

(a) amplitude (b) phase

Figure 14. Measured (experiment) and predicted (best-knowledge $u^{\text{bk},\tilde{\mu}}$ and parameterized-background data-weak estimate $u^*_{N=10,M=15}$) frequency responses at $x^{\text{c}}_m = (9.33, 2.67, 4.50)$. (a) Amplitude. (b) Phase.

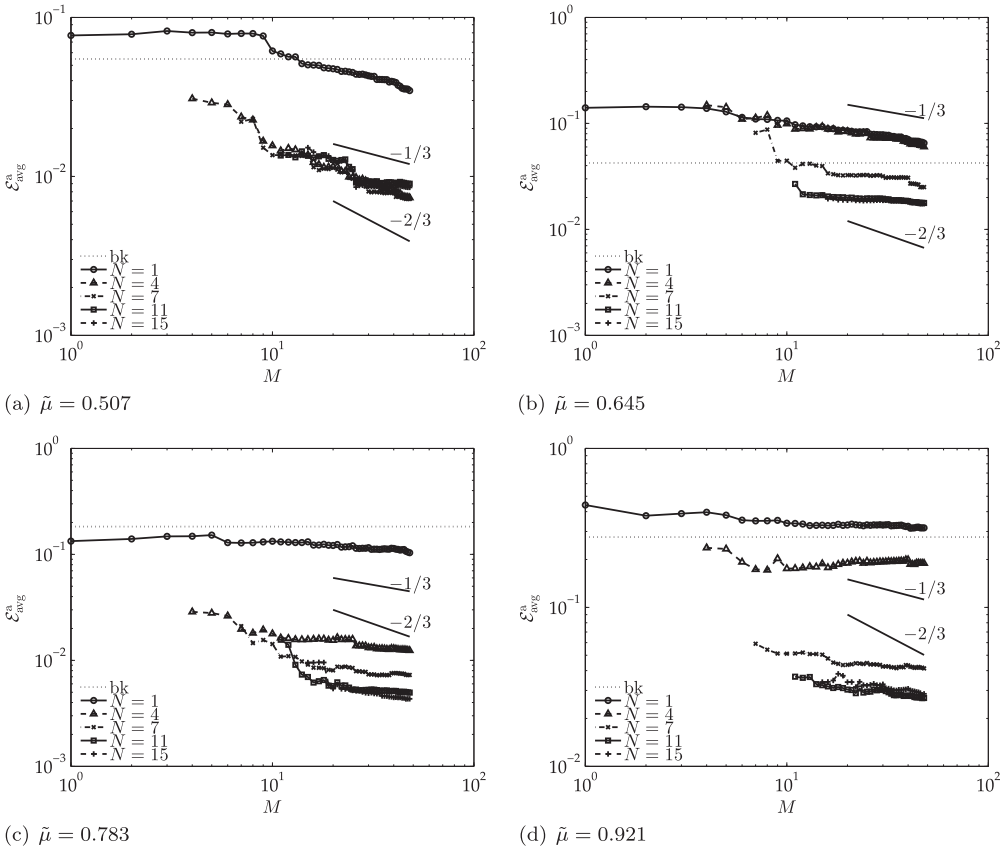

(a) $\tilde{\mu} = 0.507$ (b) $\tilde{\mu} = 0.645$

(c) $\tilde{\mu} = 0.783$ (d) $\tilde{\mu} = 0.921$

Figure 15. The variation in the error with the background space dimension N and the number of observations M at four different frequencies. (a) $\tilde{\mu} = 0.507$. (b) $\tilde{\mu} = 0.645$. (c) $\tilde{\mu} = 0.783$. (d) $\tilde{\mu} = 0.921$.

DOI: 10.1002/nme

requires less than 0.1 ms on a laptop. The total online time is thus dictated by the time for online data acquisition and is approximately $3M$ s, where M is the number of observations.

4.6. Assessment

We compare the predicted and observed (complex) pressures at 36 assessment points not chosen by the $\mathbf{SGREEDY}_{M=48}$ procedure: $\Xi^{\mathrm{a}} = \Xi \setminus \Xi_{\mathbf{SGREEDY}_{M=48}}$. We first introduce $\tilde{\mu} = \tilde{k}$ to reflect the connection between the measured/specified frequency—which shall denote the system configuration—and the parameter μ of our best-knowledge model. We then compare the best-knowledge estimate, the PBDW estimate, and the truth defined by

$$\begin{aligned} P^{\mathrm{bk}}(m;\tilde{\mu}) &= \mathrm{Gauss}(u^{\mathrm{bk},\mu=\tilde{\mu}}; x_m^{\mathrm{c,a}}, 0.2) \\ P^*_{N,M}(m;\tilde{\mu}) &= \mathrm{Gauss}(u^*_{N,M}; x_m^{\mathrm{c,a}}, 0.2) \\ P^{\mathrm{true}}(m;\tilde{\mu}) &= \{\text{normalized experimental pressure observation for mic at } x = x_m^{\mathrm{c,a}}\} \\ &\equiv \mathrm{Gauss}(u^{\mathrm{true}}; x_m^{\mathrm{c,a}}), \end{aligned}$$

respectively. Note that $\tilde{\mu}$ is not in any way utilized in the PBDW data assimilation process; the $\tilde{\mu}$ argument in $P^*_{N,M}(m;\tilde{\mu})$ is a label for the particular set of observations that inform the state estimation procedure.

A typical frequency response obtained at an assessment point is shown in Figure 14. The PBDW estimate, using a $N = 10$ background space and $M = 15$ experimental observations, provides a more accurate prediction of the truth than the best-knowledge estimate.

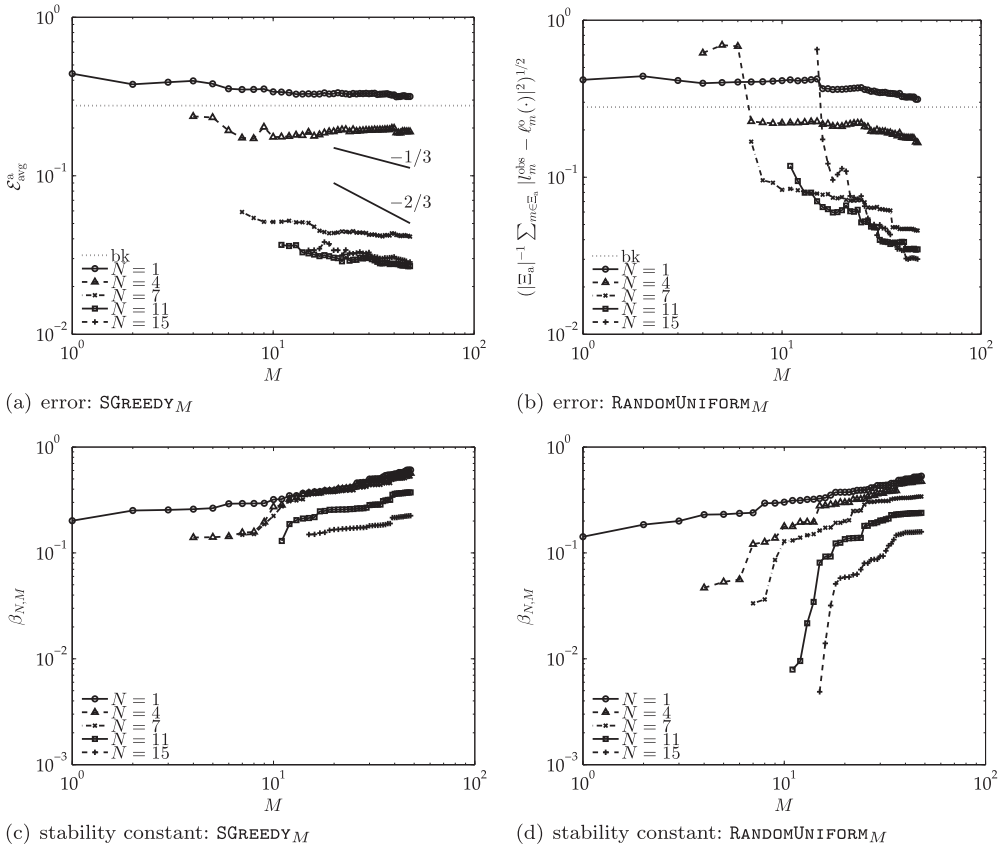

(a) error: $\mathrm{SGREEDY}_M$ (b) error: $\mathrm{RANDOMUNIFORM}_M$

(c) stability constant: $\mathrm{SGREEDY}_M$ (d) stability constant: $\mathrm{RANDOMUNIFORM}_M$

Figure 16. Behavior of the error and stability constant as a function of M and N for two different sets of observation points ($\tilde{\mu} = 0.921$). (a) Error: $\mathbf{SGREEDY}_M$. (b) Error: $\mathbf{RANDOMUNIFORM}_M$. (c) Stability constant: $\mathbf{SGREEDY}_M$. (d) Stability constant: $\mathbf{RANDOMUNIFORM}_M$.

DOI: 10.1002/nme

To assess the behavior of the PBDW estimate in more detail, we show in Figure 15 the variation in the (normalized) ℓ^2 norm of the error over Ξ^{a},

$$\mathcal{E}^{\mathrm{a}}_{\mathrm{avg}} \equiv \left(\frac{1}{M^{\mathrm{a}}} \sum_{m=1}^{M^{\mathrm{a}}} |l^{\mathrm{obs}}_m - \ell^{\mathrm{o}}_m(\cdot)|^2 \right)^{1/2},$$

as a function of the dimension of the background space N and the number of observations M at select frequencies. We recall that $M^{\mathrm{a}} = |\Xi^{\mathrm{a}}| = 36$ and the assessment set provides a good coverage of the domain Ω; hence, the discrete sum serves as an approximation of the $L^2(\Omega)$ error. We observe that the error decreases rapidly with N and slowly (but steadily) with M.

We finally compare, similar to the synthetic case, the results obtained using two different sets of observation points: the points selected by the $\textsc{SGreedy}_M$ and $\textsc{RandomUniform}_M$. We compare the estimated errors in Figure 16(a, b); we observe that the error is smaller for $\textsc{SGreedy}_M$ than for $\textsc{RandomUniform}_M$, especially when M is close to N. We then compare the stability constants in Figures 16(c, d); we observe that the $\textsc{SGreedy}_M$ provides better stability than the $\textsc{RandomUniform}_M$, and this likely results in the improved state estimate. We hence conclude that, even in the real-data setting, we benefit from the algorithms informed by the theory developed in the weak variational framework.

5. CONCLUSIONS AND PERSPECTIVES

We propose a PBDW formulation of the variational data assimilation problem for real-time and *in situ* state estimation. The formulation provides a number of contributions: 'actionable' theory—in particular the *a priori* error bounds—that identifies the criteria for the selection of the background spaces $\mathcal{Z}_N$ and update spaces $\mathcal{U}_M$; the high computational efficiency achieved through an 'optimal' selection of the background space $\mathcal{Z}_N$ from the parametric manifold by $\textsc{Process}^{\mathcal{Z}}_N$, an 'optimal' selection of the observation functionals and the associated updated space $\mathcal{U}_M$ by $\textsc{Process}^{\mathcal{U}}_M$, and real-time online computation provided by the saddle system of the size $\mathcal{O}(M)$; and simplicity and generality provided by the absence of the mathematical model in the online stage.

We demonstrate the features of the approach in a two-dimensional synthetic example; we then assess the effectiveness of the approach applied to a physical acoustic resonator. The state estimate converges rapidly with the background space dimension N if the parametric manifold of anticipated uncertainty captures the dominant features in the true state; the state estimate still converges (albeit slowly) with the update space dimension M even if the true state exhibits features not reflected in the parametric manifold.

We are currently seeking a number of extensions to the existing PBDW framework in terms of the class of problems, methodology, and physical domain. In terms of the class of problems, we are extending the framework to time-dependent problems and nonlinear problems. The treatment of time-dependent problems is based on the space–time variational formulation and analysis, through which we encapsulate, in the background space, the space–time structure of the evolutionary equation. The stability of the data assimilation procedure is then reflected in the space–time inf-sup constant, and hence, in the selection of sensors and the construction of the update space, we control the inf-sup constant while considering the limitations imposed by the particular space–time data acquisition procedure. Once we form the space–time background and update spaces in the offline stage, we then solve the saddle system in the online stage as in the steady case considered in this paper. The treatment of nonlinear problems requires the solution of an appropriate nonlinear PDE in the offline stage to construct the background spaces; however, once the state behavior is encoded in the background space, we may readily apply the construction of the saddle problem considered in this paper, as the PBDW formulation does not require the mathematical model in the online stage.

We are also pursuing various technical extensions to the PBDW framework. Here, we list a few: incorporation of available experimental data in the construction of the background space; treatment of noisy experimental observations (as described in [18] for an earlier variant of PBDW);

DOI: 10.1002/nme

an 'extracted domain approach', which introduces 'artificial' parameterized Dirichlet conditions to focus the data assimilation effort to a local region of interest [15, 30]; spatial domain decomposition approaches in which we extend the extracted domain approach to reflect continuity information between (multiple) subdomains; and parameter estimation. In particular, in the presence of noisy observations, our update $\eta^*_{N,M}$ can no longer estimate the contributions from the unanticipated uncertainties even in the limit of $M \to \infty$; we nevertheless obtain a stable estimate whose asymptotic error threshold depends on the noisiness of the data.

Finally, we are pursuing application of the PBDW framework to physical phenomena beyond acoustics: elasticity, heat transfer, fluid flow, to name a few. The relevant problems in each physical domain brings about new challenges; we wish to address these challenges through various technical extensions, some of which we have listed earlier.

ACKNOWLEDGEMENTS

We thank (in alphabetical order) Prof. Albert Cohen of Paris6, Dr. Luca Dedé of EPFL, Prof. Pierre Lermusiaux of MIT, and Tommaso Taddei of MIT for fruitful discussions. This work was supported by Foundation Sciences Mathématiques de Paris, OSD/AFOSR/MURI grant FA9550-09-1-0613, ONR grant N00014-11-1-0713, and the MIT–Singapore International Design Center.

REFERENCES

1. Fisher M. Assimilation algorithms, ECMWF NWP-DA Training Course, 2013, Reading, UK.
2. Barrault M, Maday Y, Nguyen NC, Patera AT. An "empirical interpolation" method: application to efficient reduced-basis discretization of partial differential equations. *Comptes Rendus de l'Académie des Sciences—Series I* 2004; **339**:667–672.
3. Rozza G, Huynh DBP, Patera AT. Reduced basis approximation and *a posteriori* error estimation for affinely parametrized elliptic coercive partial differential equations—application to transport and continuum mechanics. *Archives of Computational Methods in Engineering* 2008; **15**(3):229–275.
4. Porsching TA. Estimation of the error in the reduced basis method solution of nonlinear equations. *Mathematics of Computation*; **45**(172):487–496.
5. Binev P, Cohen A, Dahmen W, DeVore R, Petrova G, Wojtaszczyk P. Convergence rates for greedy algorithms in reduced basis methods. *SIAM Journal on Mathematical Analysis* 2011; **43**:1457–1472.
6. Bennett AF. Array design by inverse methods. *Progress in Oceanography* 1985; **15**:129–156.
7. Kunisch K, Volkwein S. Galerkin proper orthogonal decomposition methods for parabolic problems. *Numerische Mathematik* 2001; **90**(1):117–148.
8. Fink JP, Rheinboldt WC. On the error behavior of the reduced basis technique for nonlinear finite element approximations. *ZAMM—Journal of Applied Mathematics and Mechanics/Zeitschrift fr Angewandte Mathematik und Mechanik* 1983; **63**(1):21–28.
9. Hetmaniuk U, Tezaur R, Farhat C. An adaptive scheme for a class of interpolatory model reduction methods for frequency response problems 2013; **93**:1109–1124.
10. Maday Y, Mula O. A generalized empirical interpolation method: application of reduced basis techniques to data assimilation. In *Analysis and numerics of partial differential equations*, Brezzi F, Franzone PC, Gianazza U, Gilardi G (eds). Springer-Verlag: Milan, 2013; 221–235.
11. Patera AT, Rønquist EM. Regression on parametric manifolds: estimation of spatial fields, functional outputs, and parameters from noisy data. *Comptes Rendus de l'Académie des Sciences Paris—Series I* 2012; **350**:543–547.
12. Nguyen NC, Peraire J. An interpolation method for the reconstruction and recognition of face images. In *Visapp (2)*, Ranchordas A, Araújo H, Vitrià J (eds). INSTICC—Institute for Systems and Technologies of Information, Control and Communication: Barcelona, 2007; 91–96.
13. Everson R, Sirovich L. Karhunen-Loève procedure for Gappy data. *Journal of the Optical Society of America A* 1995; **12**(8):1657–1664.
14. Willcox K. Unsteady flow sensing and estimation via the Gappy proper orthogonal decomposition. *Computers & Fluids* 2006; **35**(2):208–226.
15. Cohen A, Davenport M, Leviatan D. On the stability and accuracy of least-squares approximations. *Foundations of Computational Mathematics* 2013; **13**:819–834.
16. Moor BD. Structured total least squares and l_2 approximation problems. *Linear Algebra and Its Applications* 1993; **188–189**:163–205.
17. Lorenc AC. A global three-dimensional multivariate statistical interpolation scheme. *Monthly Weather Review* 1981; **109**:701–721.
18. Yano M, Penn JD, Patera AT. A model-data weak formulation for simultaneous estimation of state and bias. *Comptes Rendus Mathematique* 2013; **351**(23–24):937–941.

DOI: 10.1002/nme

19. Li ZL, Navon IM. Optimality of variational data assimilation and its relationship with the Kalman filter and smoother. *Quarterly Journal of the Royal Meteorological* 2001; **127**:661–683.
20. Kalman RE. A new approach to linear filtering and prediction problems. *Transactions of the ASME—Journal of Basic Engineering* 1960; **82**(Series D):35–45.
21. Quarteroni A, Valli A. *Numerical Approximation of Partial Differential Equations*. Springer: New York, 1997.
22. Franceschini G, Macchietto S. Model-based design of experiments for parameter precision: state of the art. *Chemical Engineering Science* 2008; **63**:4846–4872.
23. Taddai T. Private communication, Jan. 2014.
24. Antoni J. A Bayesian approach to sound source reconstruction: optimal basis, regularization, and focusing. *Journal of the Acoustical Society of America* 2012; **131**:2873–2890.
25. Buffa A, Maday Y, Patera AT, Prud'homme C, Turinici G. A priori convergence of the greedy algorithm for the parametrized reduced basis method. *Mathematical Modelling and Numerical Analysis* 2012; **46**:595–603.
26. DeVore R, Petrova G, Wojtaszczyk P. Greedy algorithms for reduced basis in Banach spaces. *Constructive Approximation* 2013; **37**:455–466.
27. Ladevèze P, Chamoin L. On the verification of model reduction methods based on the proper generalized decomposition. *Computer Methods in Applied Mechanics and Engineering* 2011; **200**:2032–2047.
28. Maday Y, Mula O, Patera AT, Yano M. The generalized Empirical Interpolation Method: stability theory on Hilbert spaces with an application to the Stokes equation. *Computer Methods in Applied Mechanics and Engineering*. submitted.
29. Maday Y, Patera AT, Rovas DV. A blackbox reduced-basis output bound method for noncoercive linear problems. In *Studies in Mathematics and Its Applications*, Cioranescu D, Lions JL (eds). Elsevier Science BV: Amsterdam, 2002; 533–569.
30. Chardon G, Cohen A, Daudet L. Sampling and reconstruction of solutions to the Helmholtz equation. *Sampling Theory in Signal and Image Processing* 2013:submitted.

DOI: 10.1002/nme